

## The transcriptome of lung tumor-infiltrating dendritic cells reveals a tumor-supporting phenotype and a microRNA signature with negative impact on clinical outcome

Lotte Pyfferoen, Elisabeth Brabants, Celine Everaert, Nancy De Cabooter, Kelly Heyns, Kim Deswarte, Manon Vanheerswyngheles, Sofie De Prijck, Glenn Waegemans, Melissa Dullaers, Hamida Hammad, Olivier De Wever, Pieter Mestdagh, Jo Vandesompele, Bart N. Lambrecht & Karim Y. Vermaelen

**To cite this article:** Lotte Pyfferoen, Elisabeth Brabants, Celine Everaert, Nancy De Cabooter, Kelly Heyns, Kim Deswarte, Manon Vanheerswyngheles, Sofie De Prijck, Glenn Waegemans, Melissa Dullaers, Hamida Hammad, Olivier De Wever, Pieter Mestdagh, Jo Vandesompele, Bart N. Lambrecht & Karim Y. Vermaelen (2017) The transcriptome of lung tumor-infiltrating dendritic cells reveals a tumor-supporting phenotype and a microRNA signature with negative impact on clinical outcome, *Oncoimmunology*, 6:1, e1253655, DOI: [10.1080/2162402X.2016.1253655](https://doi.org/10.1080/2162402X.2016.1253655)

**To link to this article:** <http://dx.doi.org/10.1080/2162402X.2016.1253655>



© 2017 The Author(s). Published with license by Taylor & Francis Group, LLC© Lotte Pyfferoen, Elisabeth Brabants, Celine



Everaert, Nancy De Cabooter, Kelly Heyns, Kim Deswarte, Manon Vanheerswyngheles, Sofie De Prijck, Glenn Waegemans, Melissa Dullaers, Hamida Hammad, Olivier De Wever, Pieter Mestdagh, Jo Vandesompele, Bart N. Lambrecht, and Karim Y. Vermaelen.  
Accepted author version posted online on Nov 20 2016.  
Published online 09 Nov 2016.



Article views: 354



View supplementary material [↗](#)



Submit your article to this journal [↗](#)



View related articles [↗](#)



View Crossmark data [↗](#)

ORIGINAL RESEARCH

 OPEN ACCESS

## The transcriptome of lung tumor-infiltrating dendritic cells reveals a tumor-supporting phenotype and a microRNA signature with negative impact on clinical outcome

Lotte Pyfferoen<sup>a,b,\*</sup>, Elisabeth Brabants<sup>a,\*</sup>, Celine Everaert<sup>id c</sup>, Nancy De Cabooter<sup>a</sup>, Kelly Heyns<sup>a</sup>, Kim Deswarte<sup>b</sup>, Manon Vanheerswyngheles<sup>b</sup>, Sofie De Prijck<sup>b</sup>, Glenn Waegemans<sup>d</sup>, Melissa Dullaers<sup>id a,b</sup>, Hamida Hammad<sup>b</sup>, Olivier De Wever<sup>d</sup>, Pieter Mestdagh<sup>c</sup>, Jo Vandesompele<sup>id c</sup>, Bart N. Lambrecht<sup>b,e</sup>, and Karim Y. Vermaelen<sup>a</sup>

<sup>a</sup>Tumor Immunology Laboratory, Department of Respiratory Medicine, Ghent University Hospital, Ghent, Belgium; <sup>b</sup>VIB Inflammation Research Center, Ghent, Belgium; <sup>c</sup>Center for Medical Genetics, Ghent University, Ghent, Belgium; <sup>d</sup>Laboratory of Experimental Cancer Research, Ghent University, Ghent, Belgium; <sup>e</sup>Department of Pulmonary Medicine, Erasmus University Medical Center Rotterdam, Rotterdam, the Netherlands

### ABSTRACT

Targeting immunomodulatory pathways has ushered a new era in lung cancer therapy. Further progress requires deeper insights into the biology of immune cells in the lung cancer micro-environment.

Dendritic cells (DCs) represent a heterogeneous and highly plastic immune cell system with a central role in controlling immune responses. The intratumoral infiltration and activation status of DCs are emerging as clinically relevant parameters in lung cancer.

In this study, we used an orthotopic preclinical model of lung cancer to dissect how the lung tumor micro-environment affects tissue-resident DCs and extract novel biologically and clinically relevant information.

Lung tumor-infiltrating leukocytes expressing generic DC markers were found to predominantly consist of CD11b<sup>+</sup> cells that, compare with peritumoral lung DC counterparts, strongly overexpress the T-cell inhibitory molecule PD-L1 and acquire classical surface markers of tumor-associated macrophages (TAMs). Transcriptome analysis of these CD11b<sup>+</sup> tumor-infiltrating DCs (TIDCs) indicates impaired antitumoral immunogenicity, confirms the skewing toward TAM-related features, and indicates exposure to a hypoxic environment. In parallel, TIDCs display a specific microRNA (miRNA) signature dominated by the prototypical lung cancer oncomir miR-31. *In vitro*, hypoxia drives intrinsic miR-31 expression in CD11b<sup>+</sup> DCs. Conditioned medium of miR-31 overexpressing CD11b<sup>+</sup> DCs induces pro-invasive lung cancer cell shape changes and is enriched with pro-metastatic soluble factors. Finally, analysis of TCGA datasets reveals that the TIDC-associated miRNA signature has a negative prognostic impact in non-small cell lung cancer.

Together, these data suggest a novel mechanism through which the lung cancer micro-environment exploits the plasticity of the DC system to support tumoral progression.

**Abbreviations:** DC, dendritic cell; DC-CM, dendritic cell conditioned medium; FACS, fluorescence-activated cell sorting; GSEA, gene-set enrichment analysis; HIF, hypoxia-inducible factor; LLC, Lewis Lung Carcinoma; MDSC, myeloid-derived suppressor cell; miR(NA), microRNA; PD-L1, programmed cell death ligand 1; RT-qPCR, reverse transcription quantitative PCR; TAM, tumor associated macrophage; TCGA, The Cancer Genome Atlas; TIDC, tumor infiltrating dendritic cell; TME, tumor micro-environment; Treg, regulatory T cell; VEGF, vascular-endothelial growth factor

### ARTICLE HISTORY

Received 10 August 2016  
Revised 23 September 2016  
Accepted 24 October 2016



### KEYWORDS


Dendritic cell; hypoxia; lung cancer; miR-31; PD-L1

### Introduction

Lung cancer is the leading cause of cancer death worldwide and is characterized by a high incidence of relapse after surgical removal, along with notorious resistance toward chemotherapy and/or radiotherapy. Recently, drugs interfering with T-cell-suppressing checkpoint molecules (e.g., PD-1/PD-L1) have produced unprecedented therapeutic benefits, thereby, signaling a paradigm shift in the

treatment of this malignancy. Although these compounds can achieve long-lasting remissions in metastatic disease, this only applies to a minority of patients. This indicates that immune checkpoint molecules are but a part of the larger network of immunosuppressive mechanisms operating in lung cancer, and warrants continued efforts to map the startling complexity of the tumor-associated immune compartment.

**CONTACT** Karim Y. Vermaelen  [karim.vermaelen@ugent.be](mailto:karim.vermaelen@ugent.be)  Tumor Immunology Laboratory, Department of Respiratory Medicine, Ghent University Hospital, 9000 Ghent, Belgium.

 Supplemental data for this article can be accessed on the [publisher's website](#).

\*These authors contributed equally to this work.

Published with license by Taylor & Francis Group, LLC © Lotte Pyfferoen, Elisabeth Brabants, Celine Everaert, Nancy De Cabooter, Kelly Heyns, Kim Deswarte, Manon Vanheerswyngheles, Sofie De Prijck, Glenn Waegemans, Melissa Dullaers, Hamida Hammad, Olivier De Wever, Pieter Mestdagh, Jo Vandesompele, Bart N. Lambrecht, and Karim Y. Vermaelen.

This is an Open Access article distributed under the terms of the Creative Commons Attribution-Non-Commercial License (<http://creativecommons.org/licenses/by-nc/3.0/>), which permits unrestricted non-commercial use, distribution, and reproduction in any medium, provided the original work is properly cited. The moral rights of the named author(s) have been asserted.

Immune cells infiltrating tumor beds comprise on the one hand immunogenic/antitumoral leukocytes such as type-1-polarized macrophages and T-helper lymphocytes, cytotoxic T lymphocytes, mature dendritic cells (DCs), and natural killer cells. On the other hand, a plethora of immuno-suppressive/tumor-supporting leukocytes including regulatory T cells (Tregs), tumor-associated/M2-polarized macrophages (TAMs) and myeloid-derived suppressor cells (MDSCs) are co-opted by cancer to evade immunological destruction.

DCs are recognized as central orchestrators of immune responses in general and antitumoral immunity in particular.<sup>1</sup> In the context of cancer, DCs are capable of taking up and processing apoptotic and necrotic tumor fragments, while undergoing activation/maturation by tumor-derived innate danger signals, and present tumor-antigens to antigen-specific helper and cytotoxic T cells.<sup>2</sup> In this interaction, the mature DCs crucially need to display T-co-stimulatory molecules (e.g., CD40, CD86), while releasing cytokines and chemokines that will favor type-1-polarized and cytotoxic T-cell responses. A key cytokine in this process is IL-12, shown to be critical in the immune surveillance of carcinogen-induced tumors.<sup>3</sup>

Accordingly, the magnitude of mature myeloid DC infiltration in lung cancer specimen appears to have a substantial prognostic impact.<sup>4</sup> DC numbers were shown to be an independent predictor of survival and inversely correlated with intratumoral expression of VEGF, a pro-angiogenic cytokine that also suppresses DC functional maturation.<sup>5</sup> The presence of DC-LAMP<sup>+</sup> (i.e., mature) DCs in tumor-associated tertiary lymphoid aggregates was shown to be associated with the degree of cytotoxic T-cell infiltration and also conveys a strong prognostic signal in lung cancer patients.<sup>6</sup> Accordingly, low expression of IL-12 and of the co-stimulatory molecules CD80/CD86 in lymph nodes draining lung adenocarcinomas predicts a poorer outcome.

Furthermore, accumulating evidence suggests that the tumor micro-environment (TME) effectively enlists DCs to become active participants in the cancer-induced immunosuppressive network.<sup>7</sup> The majority of tumor-infiltrating DCs (TIDCs) in resected lung cancer specimen was shown to reside in an immature state, with a substantial subset expressing high levels of the T-cell paralyzing ligand PD-L1,<sup>8</sup> features predicting a tolerogenic function. Other reports have shown that TIDCs are capable of actively suppressing T-cell function through secretion of Arginase-1<sup>9</sup> or indoleamine 2,3-dioxygenase.<sup>10</sup> These signs of DC “corruption” indicate either a plasticity of these cells under the influence of the lung cancer micro-environment or a replacement of the immunogenic DCs by a myeloid cell population that shares some prototypical markers of DCs, yet exerts functions commonly ascribed to TAMs and MDSCs.<sup>11</sup> Either way, the phenotypical and functional shifts that DCs can undergo in tumors such as lung cancer deserve further research, given ongoing efforts to therapeutically target these cells *in vivo* to elicit effective antitumoral immunity.<sup>1</sup>

With this objective in mind, we optimized a preclinical model of lung cancer featuring orthotopic lung tumor growth in immunocompetent hosts, allowing us to compare DC populations from different tissue compartments in the same tumor-bearing lung. We found that, relative to peritumoral lung tissue

DCs, lung tumors are heavily infiltrated by cells sharing prototypical markers of CD11b<sup>+</sup> DCs and M2-polarized/tumor-supporting macrophages, along with high cell surface levels of PD-L1. Comparative transcriptomic analysis of lung TIDCs versus peritumoral DCs confirmed this acquisition of TAM features while also indicating exposure to a hypoxic environment. In addition, these lung TIDCs upregulate a defined miRNA signature that is partly hypoxia-driven and endows these cells with tumor-supporting functions. Finally, we show that the miRNA signature extracted from TIDCs predicts a worse outcome in patients with early-stage lung adenocarcinoma.

## Results

### ***An orthotopic, transplantable model of lung cancer recreating hallmark features of tumor-induced immunosuppression***

We optimized a transplantable, orthotopic model of lung cancer by inoculating Lewis lung carcinoma (LLC) cells into the airways of immunocompetent syngeneic C57BL/6 hosts using a non-invasive instillation technique. Following cancer cell transfer, lesions become apparent on H&E-stained sections as small tumoral aggregates within the lung parenchyma within 2 weeks, and grow to larger solitary nodules with histopathological similarity to human poorly differentiated non-small-cell lung carcinoma (Fig. 1A). Hosts succumb to local tumor invasion with a median survival of 4 weeks using an inoculum of  $1.5 \times 10^6$  LLC cells. Lung tumors can easily be dissected from peritumoral lung tissue, allowing further processing to address differential effects of the tissue micro-environment. Comparative analysis of single cell suspensions prepared from lungs of tumor-free mice, peritumoral lung and lung tumors revealed a relative enrichment of the intratumoral environment with Foxp3<sup>+</sup> Tregs, monocytic myeloid-derived suppressor cells (mo-MDSCs), along with an upregulation of the PD-1 exhaustion marker on tumor-infiltrating CD4<sup>+</sup> and CD8<sup>+</sup> T cells (Fig. 1B). Locoregional effects were also manifested as a forceful increase in Tregs as well as mo-MDSCs and granulocytic MDSCs in mediastinal lymph nodes draining tumor-bearing lungs, relative to lymph nodes of tumor-free lungs. Systemic effects were also manifested as an increase in (granulocytic) MDSCs within the spleen of orthotopic lung tumor-bearing hosts.

### ***Orthotopic lung tumors are heavily infiltrated by myeloid cells sharing generic dendritic cell markers as well as phenotypical characteristics of alternatively activated macrophages***

We examined the total DC tissue content by strictly gating on CD11c<sup>high</sup>MHCII<sup>high</sup> leukocytes after exclusion of dead cells, high autofluorescent cells (containing pulmonary macrophages), and T-/B-lymphocytes (Fig. 2A). In LLC lung tumors, we found that the leukocytic infiltrate was highly enriched with DCs when compared with adjacent peritumoral lung and naive lung (around 10-fold increase) (Fig. 2B). Lung DCs have been shown to segregate into ontogenically and functionally separate

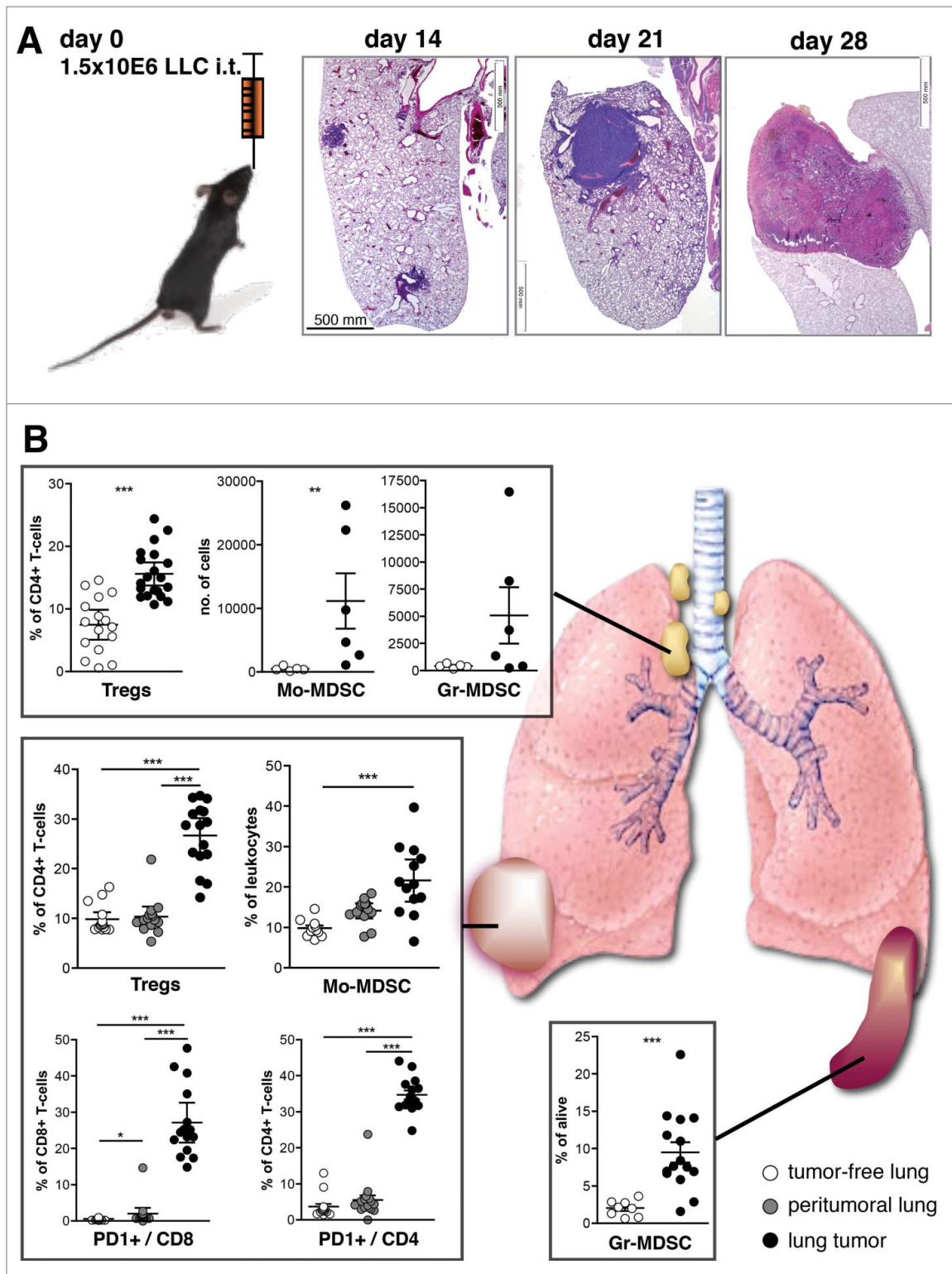


**Figure 1.** Orthotopic preclinical model of lung cancer. (A) H&E-stained sections of paraffin-embedded lungs illustrate typical early- mid- and advanced-stage intrapulmonary tumor growth. (B) Flow cytometry on single-cell suspensions from different anatomical compartments: tumor-free lung, peritumoral lung tissue, lung tumor tissue, tumor-draining mediastinal lymph nodes, and spleen. Tregs were gated as live CD4<sup>+</sup>/Foxp3<sup>+</sup> lymphocytes. PD-1 expression was assessed on the surface CD3<sup>+</sup>/CD4<sup>+</sup> and CD8<sup>+</sup> T cells. Monocytic and granulocytic MDSCs were gated as CD45<sup>+</sup>/CD11b<sup>+</sup>/Ly6C<sup>high</sup>/Ly6G<sup>low</sup> and CD45<sup>+</sup>/CD11b<sup>+</sup>/Ly6C<sup>low</sup>/Ly6G<sup>high</sup> cells, respectively. Data pooled from two independent experiments with 3–10 mice per group.

CD11b<sup>+</sup>CD103<sup>-</sup> and CD11b<sup>-</sup>CD103<sup>+</sup> subsets.<sup>12</sup> Within the orthotopic lung tumors, we observed an overwhelming predominance of the CD11c<sup>high</sup>/MHCII<sup>high</sup> CD11b<sup>+</sup> CD103<sup>-</sup> subset with a minor population of CD103<sup>+</sup>CD11b<sup>-</sup> DCs (Fig. 2C).

We further examined the phenotype of this CD11b<sup>+</sup> subset in terms of surface expression of T cell co-stimulatory and check-point receptors (Fig. 2D). Compared to peritumoral counterparts and CD11b<sup>+</sup> lung DCs from tumor-free hosts, we

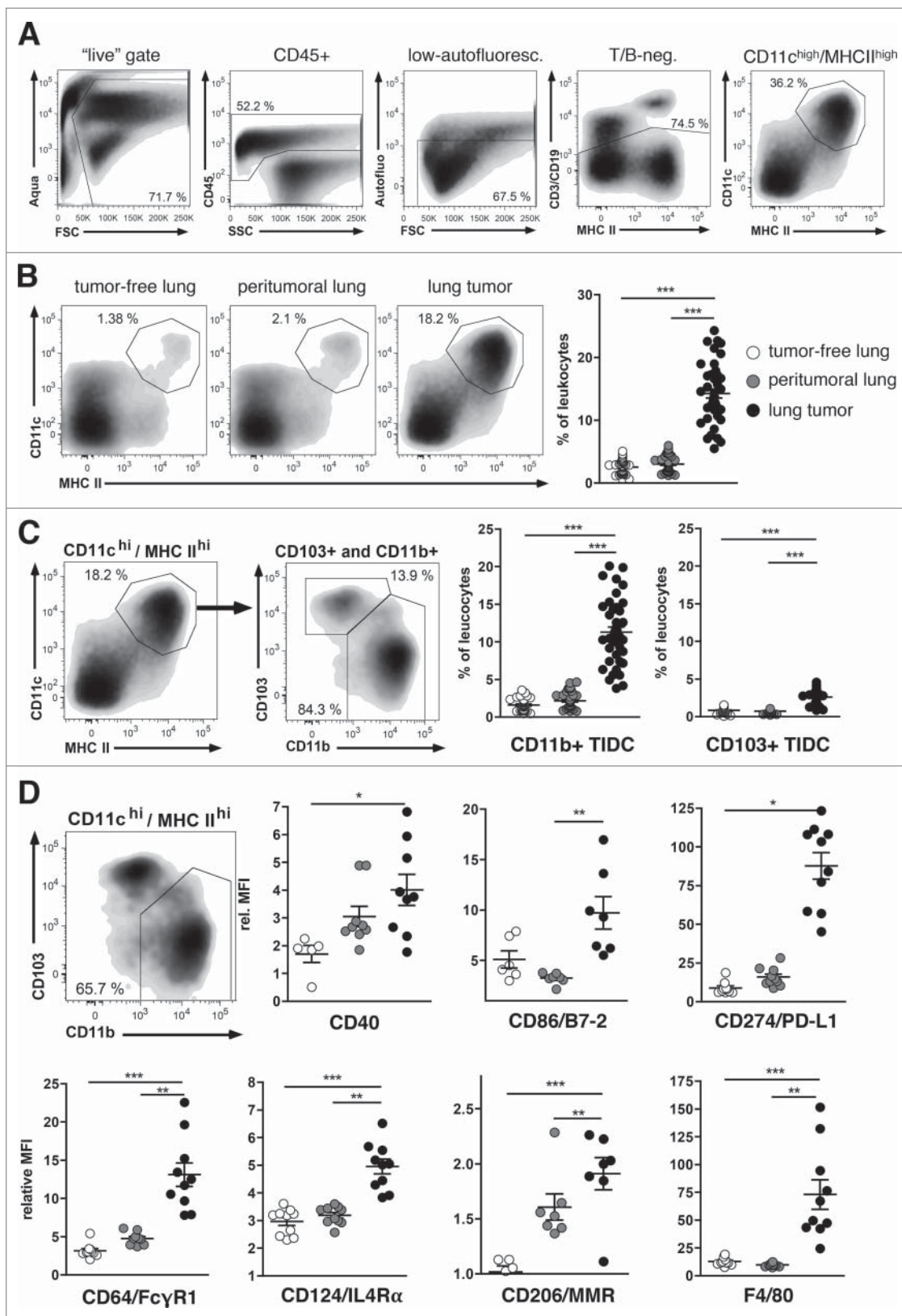


**Figure 2.** Quantitative and phenotypical analysis of the global dendritic cell infiltrate in orthotopic lung tumors. Lung tumors at day 28 after intratracheal instillation of LLCs were dissected from peritumoral lung tissue and single cell suspensions were prepared by gentle enzymatic digest for further downstream analysis. (A) Gating strategy used to delineate the DC compartment. Indicated percentages represent the frequency of immediate parent population. (B) Comparative quantitative analysis showing magnitude of DC infiltration in each tissue compartment, expressed relative to total leukocyte content. (C) Relative abundance of the CD11b<sup>+</sup>CD103<sup>-</sup> versus CD11b<sup>+</sup>CD103<sup>+</sup> DC subpopulations in tumor-free lung, peritumoral lung, and lung tumor tissue. Data pooled from six independent experiments with 5–10 mice per group. (D) Surface marker analysis of the CD11b<sup>+</sup> DC subpopulation for expression of T-cell co-stimulatory/co-inhibitory ligands and tumor-associated macrophage related markers (gating sequence as in Fig. 2A). Data shown are representative of 2–3 independent experiments with *n* = 4–9 mice per group. Bars denote mean ± SEM.

observed an upregulation of the co-stimulatory molecules CD40 and CD86, however, paralleled by a strong increase in surface expression of CD274/PD-L1. In addition, TAM markers such as F4/80, CD64/Fc $\gamma$ RI and M2-polarized macrophage markers CD206/MMR and CD124/IL4R $\alpha$  were distinctly upregulated on these cells, further referred as “TIDCs”. Representative histograms illustrating the shifts in surface marker expression are provided as Fig. S1. Surface expression of the inflammatory monocyte marker Ly6C was also increased on TIDCs, whereas the granulocytic marker Ly6G and the pulmonary macrophage marker Siglec F were not detected on these cells (data not shown).

### **The transcriptome of lung tumor-infiltrating DCs confirms a loss of immunogenic functions, the acquisition of TAM features, and cellular responses to hypoxia**

We sought to gain a deeper understanding of how the TME affects the biology of the tissue-resident DC compartment. The ability to perform comparisons between tumor-infiltrating and peritumoral cells isolated from the same host (internal control) is an inherent advantage of the orthotopic model and allows correcting for potential confounding factors. Therefore, in further comparative analyses, we focused on the differential gene expression between paired TIDCs and peritumoral DCs, focusing on the dominating CD11b<sup>+</sup> subset. We FAC-sorted pools of CD11c<sup>high</sup>/MHCII<sup>high</sup>/CD11b<sup>+</sup> leukocytes from peritumoral lung tissue ( $n = 8$ ) and paired lung tumor tissue ( $n = 7$ ), and hybridized the extracted RNA to an exon microarray (Fig. 3A). We identified significantly downregulated or upregulated genes using a cut-off of  $p < 0.001$  in combination with a fold-change cut-off of  $|\log_2(\text{foldchange})| > 1$ . We used a stringent  $p$ -value  $< 0.001$  as a form of correcting for multiple testing.<sup>13</sup> Compared to peritumoral lung CD11b<sup>+</sup> DCs, 37 genes were upregulated and 103 genes were downregulated in CD11b<sup>+</sup> TIDCs (full expression data available under accession number GSE85044) (Fig. 3B). A volcano plot of Limma-estimated  $\log_2$ -ratios versus minus the  $\log_{10}$   $p$ -value assisted us in highlighting a set of top modulated transcripts and orienting further analysis in terms of relevant biological processes (Fig. 4A). Among the 37 transcripts significantly upregulated in CD11c<sup>high</sup>/MHCII<sup>high</sup>/CD11b<sup>+</sup> TIDCs, 23 were typically expressed by M2-polarized and TAMs (matrix metalloproteinase 9, matrix metalloproteinase 8, chemokine C-C motif ligand 8, macrophage scavenger receptor-1, arginase 1, and cathepsin K) in addition to a number of generic macrophage genes such as Fc-gamma receptor 1b (CD64) and the macrophage transcription factor Tcfec, both of which also highly expressed in inflammatory monocytes ([www.immgen.org](http://www.immgen.org)). A total of 8 out of the 37 transcripts directly or indirectly reflected response to hypoxia (EGLN3/prolyl hydroxylase 3, 5'-ectonucleotidase, Blc2-and-19kD interacting protein 3, pyruvate dehydrogenase kinase 1, CCL8, and Cathepsin K). Four of which (Mmp9, CCL8, MSR1, and CTSK) are also macrophage-associated genes (Fig. 4B). Among the transcripts downregulated in lung TIDCs compared with peritumoral DCs were factors involved in promoting T helper 1 immune responses (IL-12b, IL18R1), the mouse homolog of the antigen-uptake receptor

DC-SIGN (CD209b), angiotensin-converting enzyme (ACE; shown to inhibit MDSC development)<sup>14</sup> and Gpcr5a (known to suppress inflammation-associated lung carcinogenesis).<sup>15</sup>

Based on the phenotypical, functional, and transcriptomic findings, we then proceeded to interrogate the expression data via gene-set enrichment analysis (GSEA<sup>16</sup>). To that end, we first generated comprehensive gene lists focusing on (1) DC immunogenicity, (2) M2-polarized and TAM features, and (3) cellular response to hypoxia (Table S1). Comparative GSEA of lung TIDC versus peritumoral lung DC transcriptomes showed a strong downregulation of features required for optimal DC immunogenicity and the capacity to induce type-1-polarized T-cell responses. In parallel, there was a marked enrichment for genes related to TAM and M2-polarized macrophage biology, and a distinct enrichment signature reflecting response to hypoxia (Fig. 4C).

Additional information can be accessed from the transcriptomic data by looking at activities of motifs belonging to gene promoters and the network of corresponding transcription factors (TFs). Applying Integrated Motif Activity Response Analysis (ISMARA<sup>17</sup>) on the tumor-free lung DC—peritumoral lung DC—lung TIDC dataset highlighted a list of significantly modulated motif activities (Fig. 5A and Table S2). Sorted by Z-score (i.e., the average squared ratio between fitted activities and their standard deviations), the ETS1,2.p2 motif emerged on top, with a strong downregulation of its activity in TIDCs as compared with peritumoral CD11b<sup>+</sup> DCs or DCs from tumor-free lungs. Two TFs, Ets1 & Ets2, are associated with ETS1,2.p2. However, only Ets1 showed a significant correlation between motif activity and mRNA expression of the TF itself (Pearson correlation coefficient = 0.69,  $p$ -value = 0.0004; Fig. 5B). Gene Ontology (GO) analysis on the top predicted targets of Ets1 yielded processes exclusively related to positive regulation of immune response, antigen presentation, and T-cell activation (Fig. 5C). In addition, ISMARA predicts a loss of STAT4 transcription activity in TIDCs, which is in line with the downregulation of IL12b transcripts in these cells.<sup>18,19</sup> Thus, genome-wide prediction of transcription factor activity converges with our functional data as well GSEA on lung TIDCs to indicate a decreased antigen-presenting capacity, while also predicting an impaired potential to induce type-1-polarized T-cell responses. Remarkably, motifs associated with TFs regulating response to hypoxia as well as ER-stress were situated among the top 10% in terms of activity significance (Z-score) (Fig. 5A). These included NFE2, ATF4, XBP1, NRF1, and HIF1A, the activities of which are all predicted to be upregulated in TIDCs as compared with peritumoral lung DCs. Of additional interest is the relative loss of PPAR $\gamma$  activity in TIDCs. Known to suppress myeloid cell induced systemic inflammation, immune suppression, and tumorigenesis.<sup>20</sup> PPAR $\gamma$  is also known to be negatively regulated by hypoxia. As a whole, the predicted transcriptional signature of hypoxia exposure is again in line with the GSEA.

### **A distinct pattern of microRNA expression distinguishes CD11b<sup>+</sup> lung tumor-infiltrating from peritumoral lung DCs**

In parallel to exon analysis, RNA samples from purified lung peritumoral and intratumoral CD11b<sup>+</sup> DCs were also processed for genome-wide RT-qPCR-based expression

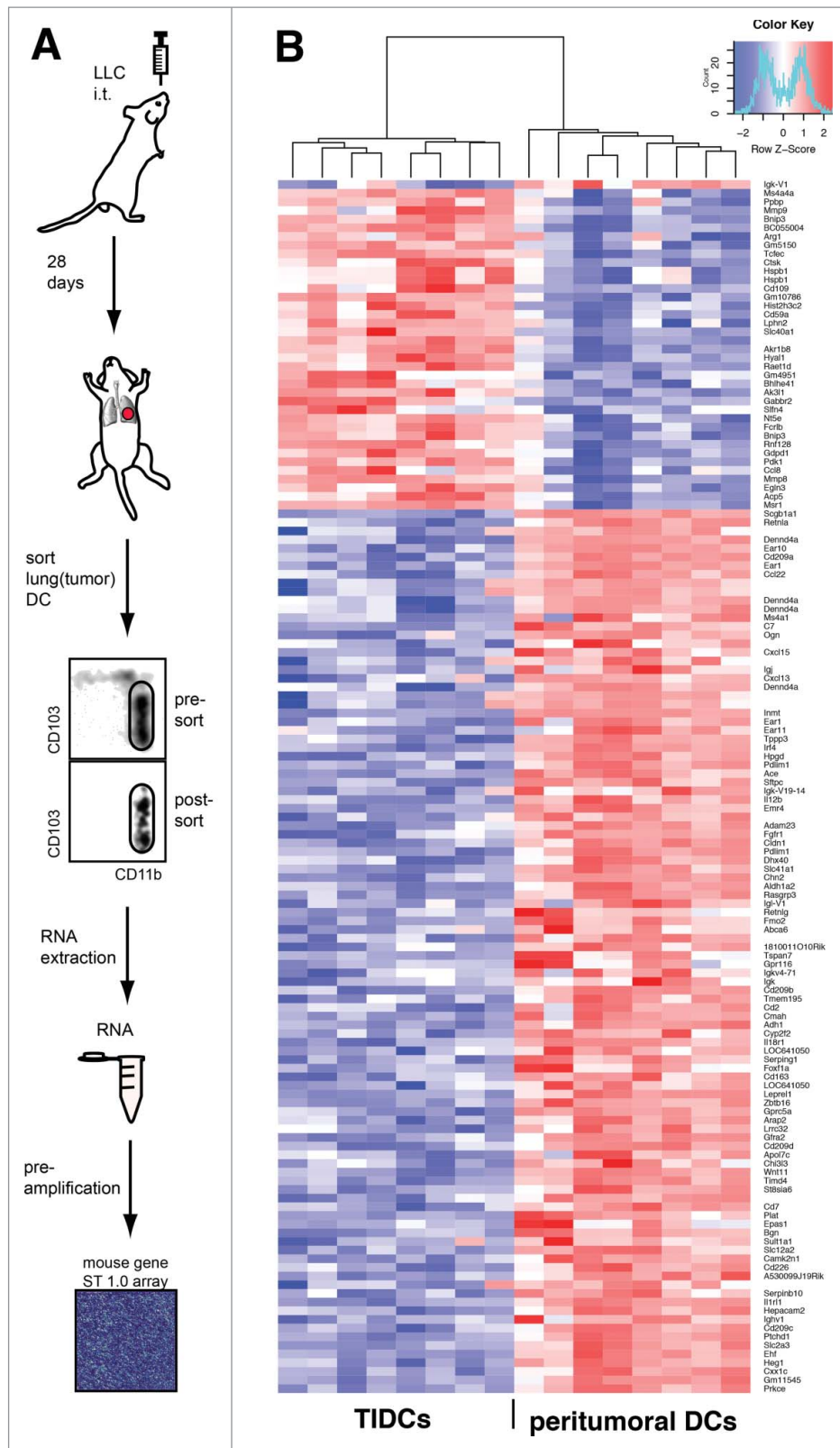


**Figure 3.** Differential gene expression in CD11b<sup>+</sup> TIDCs from lung tumor bearing mice. (A) Workflow for the generation and preparation of samples for gene expression profiling. (B) Heatmap displaying the normalized differentially expressed genes in CD11b<sup>+</sup> peritumoral lung DCs and lung tumor DCs as identified by exon array (absolute value of log<sub>2</sub> > 1 and *p* < 0.001) and hierarchical clustering of the samples. There are 7–8 replicates from two independent experiments, each replicate consisting of a pool of DCs of tumor or lung tissue from 6 to 8 mice. Rows represent modulated probes (gene name or probeID). Colors denote log<sub>2</sub>-fold expression levels.

profiling of miRNAs. We found 17 mature miRNAs to be differentially expressed in TIDCs compare with peritumoral lung DCs (*p* < 0.05; Fig. 6A). MiR-31-5p, miR-31-3p, miR-193b, miR-214-3p, and miR-127 were consistently

upregulated in TIDCs, whereas miR-126-5p, miR-126-3p, miR-218, miR-455, miR-30a-3p, miR-497, miR-9-3p, miR-138, miR-9-5p, miR-146a, miR-145, and miR-150 were downregulated in TIDCs.

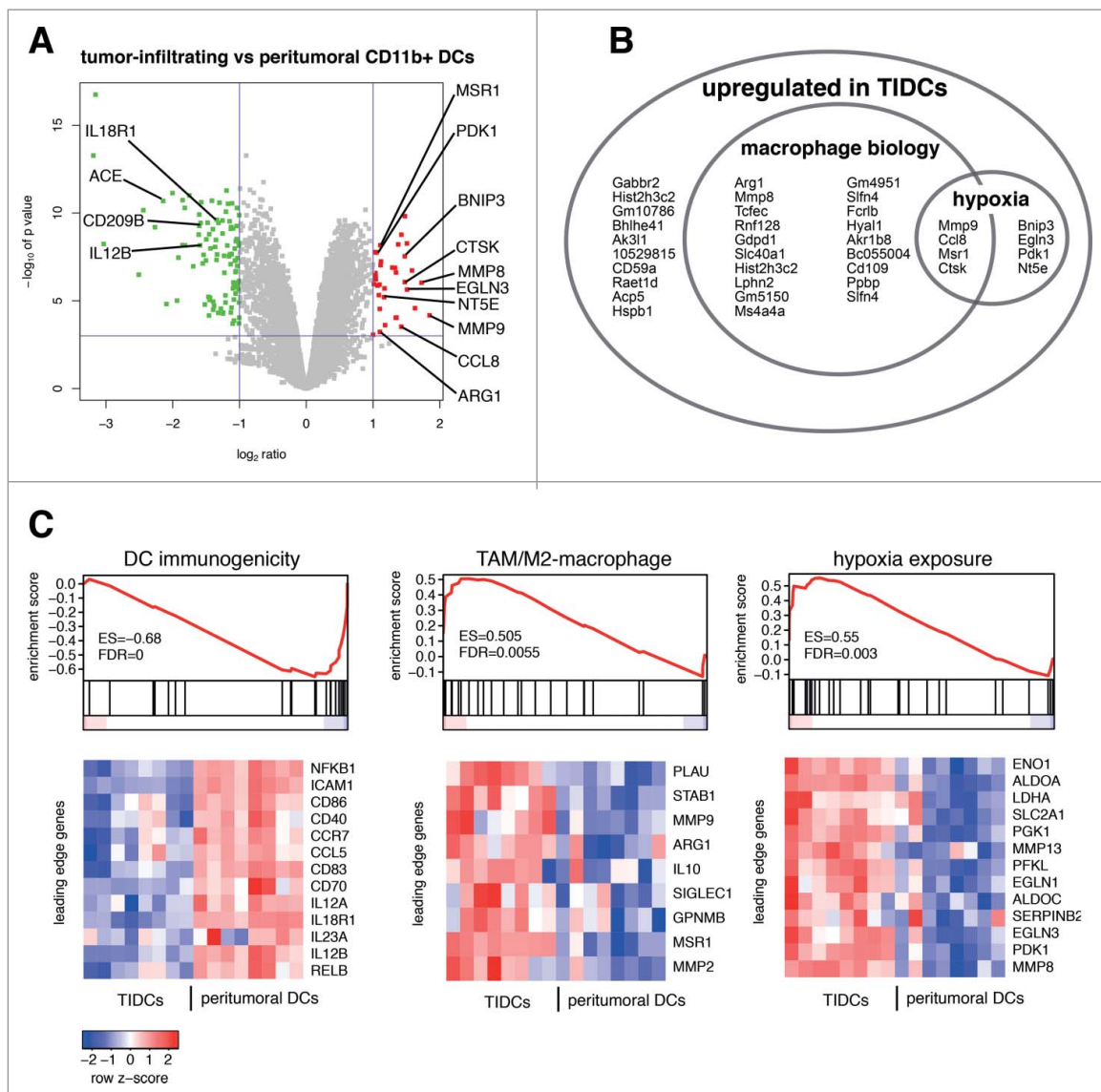


**Figure 4.** (A) Volcano plot of differential gene expression between lung tumor-infiltrating versus peritumoral lung DCs. Limma-estimated  $\log_2$ -ratios versus  $\log_{10}$   $p$ -value. (B) Functional grouping of transcripts upregulated in CD11b<sup>+</sup> tumor-infiltrating DCs versus peritumoral lung DCs. (C) Gene set enrichment analysis (GSEA, [www.broadinstitute.org/gsea/](http://www.broadinstitute.org/gsea/)) performed on the transcriptomic data, using comprehensive gene lists pertaining to DC immunogenicity (in particular the capacity to induce type-1-polarized immune responses), tumor-associated/alternatively activated macrophage features, and cellular responses to hypoxia (see also Table S1).

Remarkably, miR-31 emerged as the differentially expressed miRNA with the greatest magnitude of upregulation in lung TIDCs compare with peritumoral DCs (Fig. 6B). We detected upregulated expression of both miR-31 transcripts by RT-qPCR on FAC-sorted DCs from a separate cohort of lung tumor-bearing hosts (Fig. 6C).

#### Hypoxia drives intrinsic miR-31 expression in myeloid DCs

MiR-31 is known to be implicated in cellular responses to hypoxia by targeting FIH (factor inhibiting HIF) to de-repress HIF-1 $\alpha$ . This, together with indications derived from the mRNA expression analyses, prompted us to verify whether DCs infiltrating orthotopic lung tumors were indeed exposed to hypoxic zones. *In vivo* administration of pimonidazole allows us to specifically label hypoxic tissue regions. Using immunofluorescence labeling, we visualized the relationship between intratumoral pimonidazole staining distribution and

infiltration with CD11c-expressing cells. Imaging by confocal microscopy could consistently demonstrate co-localization of dendritic-shaped CD11c<sup>+</sup> cells within intratumoral hypoxic areas (Fig. 7A and B). Next, we wondered whether hypoxia could in itself induce miR-31 expression in DCs. We derived DCs from GM-CSF-supplemented bone marrow cell suspensions, as this generates a mixed population of CD11b<sup>+</sup> cDCs and macrophage-like DCs that are analogous to the *in vivo* TIDC cluster in our model.<sup>21,22</sup> Exposure to 1% oxygen tension, especially in combination with TLR stimulation, was sufficient to trigger a robust increase in intrinsic expression of both miR-31 transcripts in these myeloid DCs (Fig. 7C).

#### MicroRNA-31 and hypoxia endow myeloid DCs with tumor-supporting properties

We used GM-CSF-supplemented bone marrow cultures to further dissect the biological impact of miR-31 overexpression on



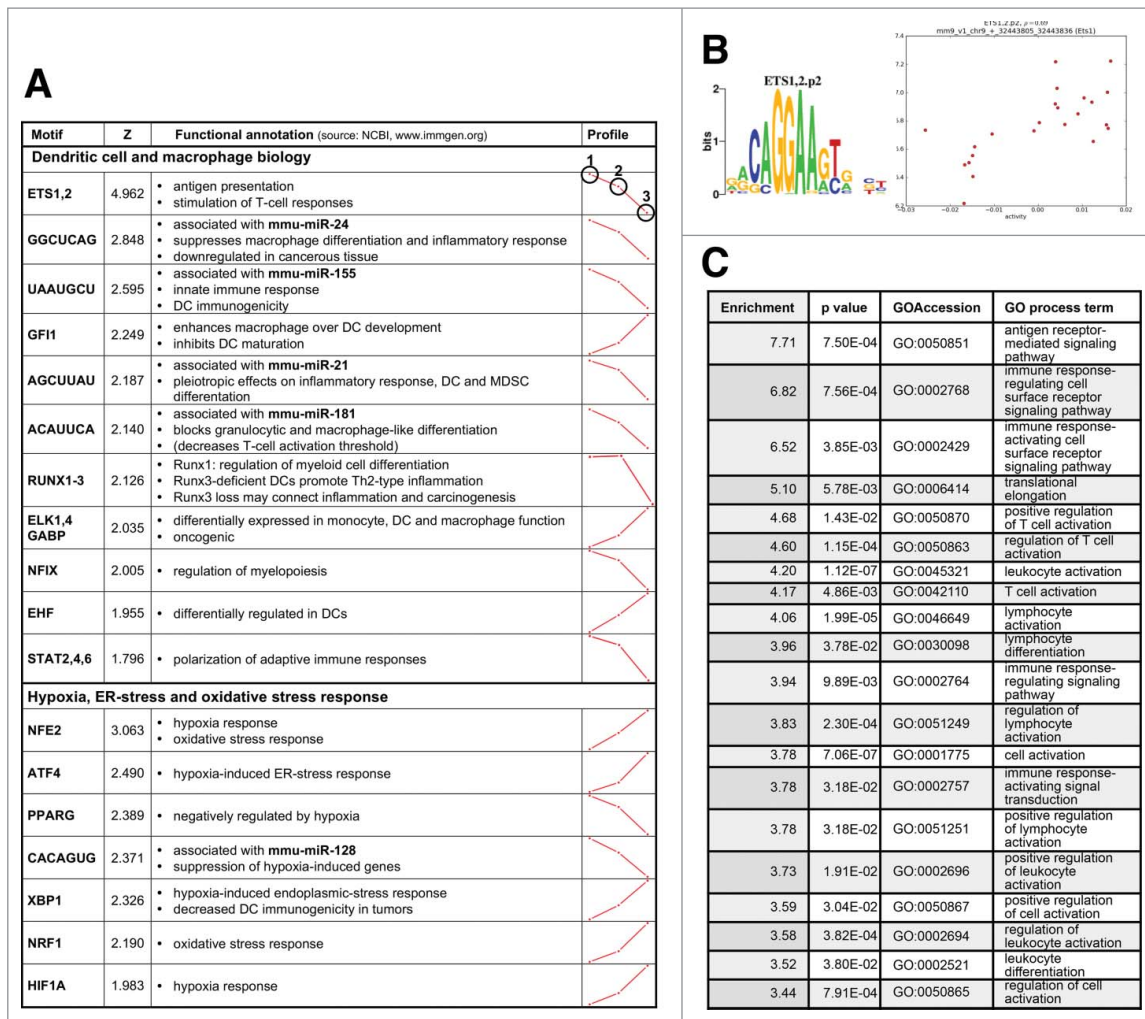


**Figure 5.** *In silico* prediction of dominant transcription factor activity. Integrated System for Motif Activity Response Analysis (ISMARA, Swiss Institute of Bioinformatics) was applied to the gene expression dataset. (A) Tabular overview of transcription factor activity showing (from left to right) motif name, activity significance (Z), functional data (source: <http://www.ncbi.nlm.nih.gov/gene>) and a graphical representation of differential regulation: CD11b<sup>+</sup> DCs from (1) lungs of tumor-free hosts, (2) peritumoral lung tissue, and (3) lung tumor tissue. The list is sorted by activity significance with a lower cut-off of Z = 1.5 (for a full list, see Table S2). (B) Focus on ETS1, 2, the motif with highest activity significance, showing (top left) motif logo, (top right) Pearson correlation plot of motif activity versus mRNA expression, which was only significant for ETS1/Ets1. (C) Gene Ontology analysis of ETS1 targets by process category.

CD11b<sup>+</sup> myeloid DCs. Unexpectedly, transfection of *in vitro* generated DCs with miR-31-5p or -3p mimics had no measurable impact on cardinal features of these cells, be it surface expression levels of T-cell co-stimulatory/co-inhibitory molecules or stimulation of antigen-specific T-cell proliferation (data not shown). Given the fact that miR-31 is involved in pro-angiogenic and pro-metastatic pathways, we thus hypothesized that miR-31 upregulation might endow CD11b<sup>+</sup> DCs with tumor-supporting properties. Using a collagen type I invasion assay, we observed that conditioned medium of miR-31-3p overexpressing DCs induces loss of cellular sphericity and the appearance of filopodia-like protrusions in lung carcinoma cells, i.e., shape changes that are indicators of invasive behavior<sup>23</sup> (Fig. 8A and B). This effect was not observed with conditioned medium of miR-31-5p overexpressing DCs. DC-conditioned medium was subsequently analyzed using a multiplex protein biomarker assay focusing on soluble factors belonging to pro-angiogenic and pro-invasive pathways. Out of 17 protein analytes in the assay, 8 were reliably detected (S100A8, S100A9, VEGF, MMP-9, HGF, osteopontin, PDGF,

and lipocalin-1). Of these, only the release of S100A8, S100A9, and VEGF by DCs was boosted by miR-31-3p overexpression and a hypoxic environment alike (Fig. 9A and B).

### The miRNA signature of lung tumor-infiltrating DCs has a marked prognostic impact in human lung adenocarcinoma

miRNA sequences are known to possess a high degree of target conservation among mammals. This offered us an opportunity to explore whether the miRNA signature contained in a “corrupt” lung tumor-associated DC population confers prognostic information in lung cancer patients. We retrieved RNA-sequencing data of non-small cell lung cancer (NSCLC) cohorts from The Cancer Genome Atlas (TCGA) portal and applied algorithms allowing to extract non-coding RNA expression information. The TCGA clinical annotation database was downloaded and updated to the latest (seventh) TNM staging system for lung cancer where necessary. A follow-up of 5 y was considered for the survival analysis and patients having developed a secondary cancer were excluded. First, our analysis

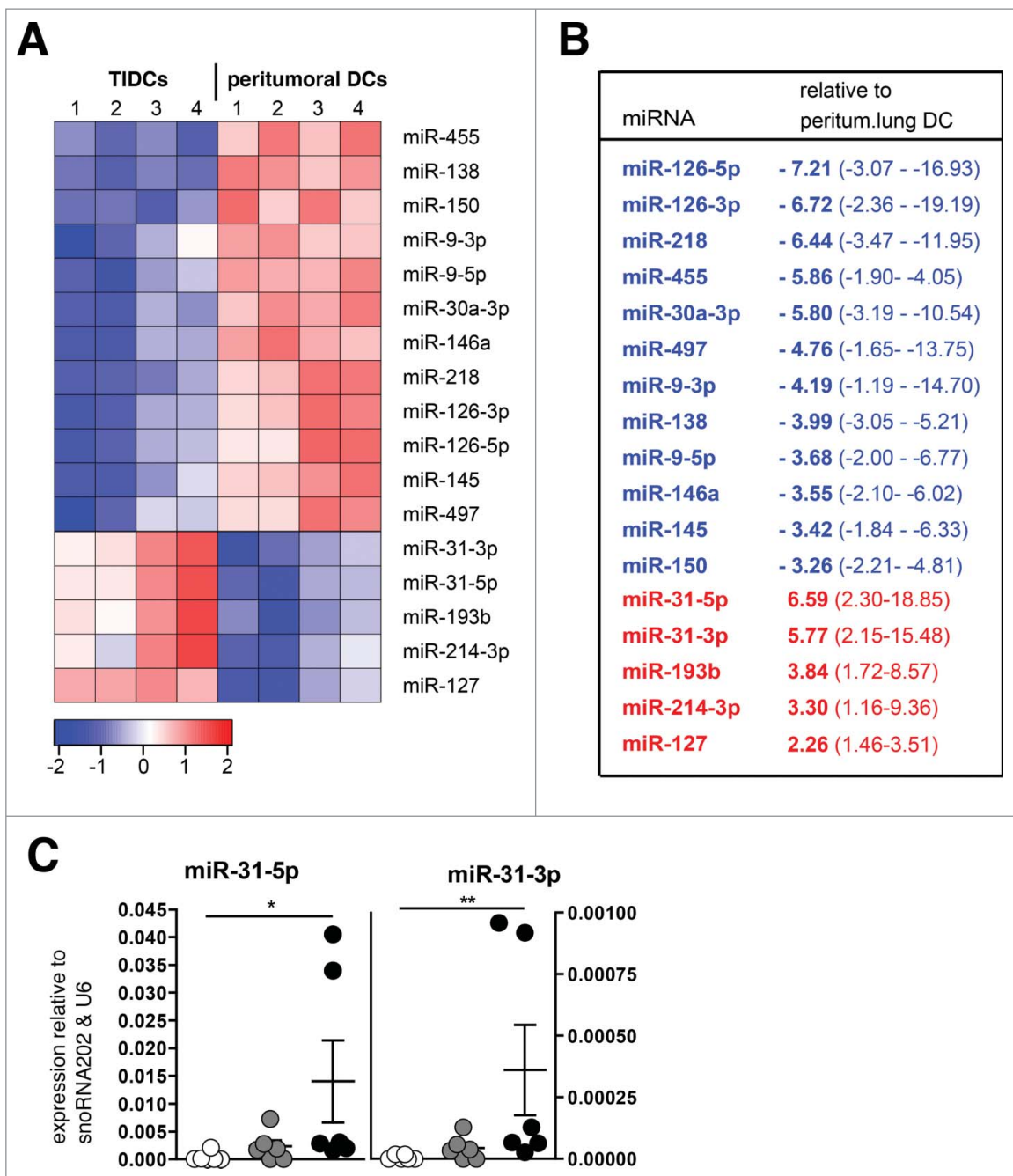


**Figure 6.** Differential miRNA expression in tumor-infiltrating and hypoxia-exposed DC. (A) Heatmap of normalized RT-qPCR values showing mature miRNA levels differentially expressed in CD11b<sup>+</sup> DCs directly isolated from lung tumor versus peritumoral lung tissue (four replicates from one experiment, each replicate the result of pooling DCs FACSsorted from lung or tumor of 6–8 mice). (B) Statistical analysis comparing relative expression levels between intra- and peri-tumoral DCs, expressed as fold change and 95% confidence interval. Rank products test with percentage of false positives < 5%. (C) Separate analysis delivering RT-qPCR-based expression levels of miR-31-5p and miR-31-3p relative to reference genes (snoRNA202 and U6) in CD11b<sup>+</sup> TIDC versus peritumoral lung tissue DCs FACSsorted 28 d post-implantation of LLC cells. Data pooled from two experiments with 2–4 replicates per group, each replicate containing pooled RNA from FAC-sorted DCs of 7–19 mice.

confirmed previous reports that suggested a negative prognostic impact of miR-31 expression on overall survival in NSCLC (across all stages) (Fig. 10A). However, the strength of the full TIDC miRNA signature showed an even greater effect on prognosis, with a median overall survival not reached in patients with low signature strength, versus 3.4 y in the early stage patient group with high signature strength. Of particular interest, the TIDC miRNA-signature specifically segregated lung cancer patients with nodal invasion (N1 and N2) into two groups with dramatically different outcome (Fig. 10B). Detailed

numerical data on median overall survival, 5-y survival rate and hazard ratio for death can be found in Table 1. These effects on outcome were only observed in the non-squamous subtype, which makes up the majority of NSCLC cases.

## Discussion

In contrast to more widely used subcutaneous transplantable tumor models, orthotopic tumor inoculation uniquely allows us to perform differential analysis of cell populations across

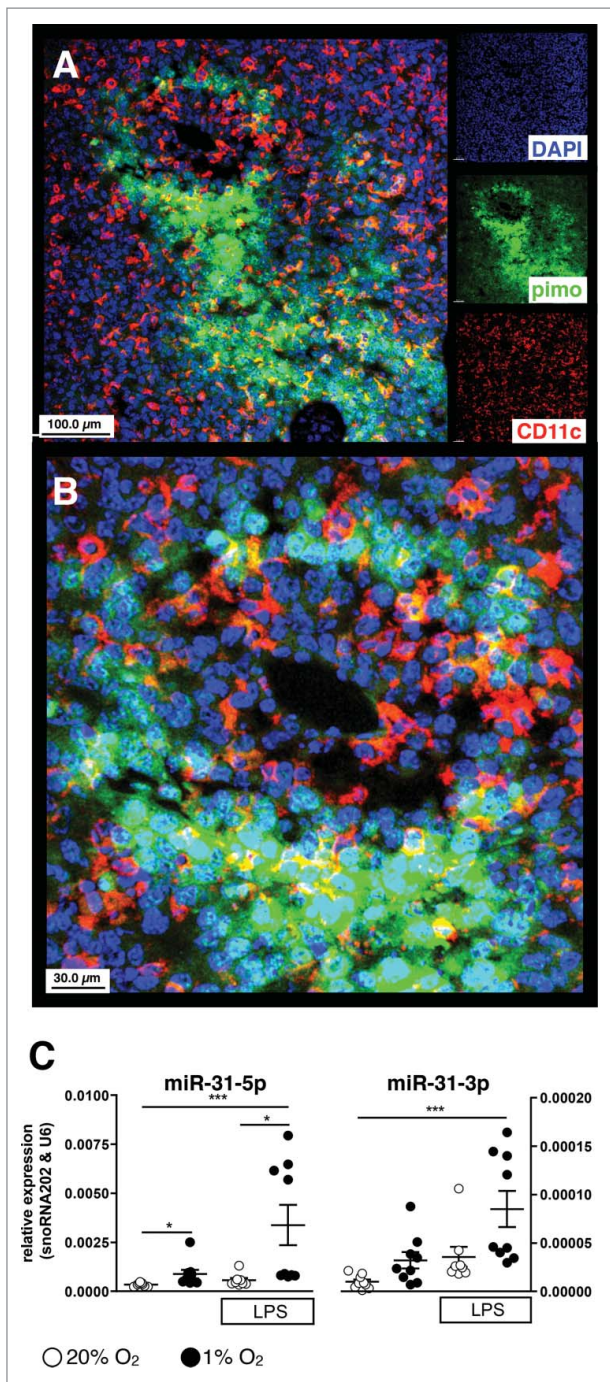


**Figure 7.** Co-localization of DC infiltration and hypoxic regions within orthotopic lung tumors. (A) Cryosection of orthotopic lung tumor from pimonidazole-injected host stained for cell nuclei (DAPI, blue), pimonidazole-adducts (green), and CD11c (red). (B) Higher power magnification focusing on a perivascular region, showing hypoxic rim at a distance from a blood vessel, and dendritic-shaped CD11c<sup>+</sup> cells. (C) Normalized RT-qPCR expression levels of miR-31-5p and miR-31-3p in day 8 bone marrow-derived DCs, exposed for 48 h to 1% O<sub>2</sub> with or without 100 ng/mL LPS for 12 h. Data pooled from two independent experiments, with each experiment involving four mice per group.

adjacent tissue compartments within the same organ. In this study, we took advantage of this opportunity to dissect how the lung TME affects the pulmonary DC compartment.

Within the lung, the conventional DC system has been shown to contain CD11b<sup>+</sup>CD103<sup>-</sup> and CD11b<sup>-</sup>CD103<sup>+</sup> subsets with dedicated immunogenic tasks.<sup>12</sup> Here, we show that within the intrapulmonary TME, the CD11c<sup>high</sup>/MHCII<sup>high</sup>/

CD11b<sup>+</sup> lung DC compartment becomes heavily infiltrated by a myeloid population displaying canonical features of alternatively activated, TAMs,<sup>24</sup> both at the immunophenotypical and transcriptomic levels. Our data are in line with a recent description of a CD11b<sup>+</sup> “DC1” being the dominant TIDC population in several mouse tumor models, and likewise co-expressing several markers belonging to TAMs such as the CD64, MMR, and MerTK.<sup>25</sup> The lung tumor TIDC in our model also shows striking similarity to the CSF-1-dependent, MMP-expressing “macrophage-DCs” described in an MMTV-PyMT/c-fms-EGFP mouse model of breast cancer.<sup>26</sup>

We did not address whether these tumor-induced shifts rely on a plasticity of lung tissue resident conventional DCs, or on a gradual replacement of this cellular compartment by newly recruited macrophage-like cells. It was previously reported that proliferating CD11c<sup>+</sup>MHCII<sup>+</sup> cDCs derived from pre-cDCs can acquire a regulatory macrophage-like phenotype when exposed to tumor-conditioned media.<sup>27</sup> However, these “DC-derived macrophages,” which are also specifically enriched within tumor beds (including ectopic LLC tumors), lose expression of CD11c and MHCII, in complete opposition to the CD11b<sup>+</sup> TIDCs we described.

A striking feature of TIDCs in our model is the intense upregulation of the inhibitory checkpoint molecule PD-L1 when compared with matched peritumoral CD11b<sup>+</sup> DCs. High expression of PD-L1 is also a prominent feature of DCs infiltrating human non-small cell lung cancer specimen (see ref. 8 and our unpublished observations). It was previously reported that monocyte-derived DCs use PD-L1 to cross-tolerize T cells to antigens derived from apoptotic cells.<sup>28</sup> Moreover, a recent study performed in a mouse model of melanoma showed that PD-L1 expression on TIDCs rather than on tumor cells contributes to immune paralysis and mediates response to PD-L1 checkpoint blockade.<sup>29</sup> This implies that DCs, which more than any other cell excel in the recruitment of, and close interaction with T cells, could act as the main focus of immune paralysis in the TME. Of note, PD-L1 on intratumoral immune cells has been validated as a strong predictive biomarker of clinical response to anti-PDL1 therapeutic antibodies across several tumors, including lung cancer.<sup>30</sup>

Moving beyond immunophenotype, our work provides a unique look into the transcriptome of DCs infiltrating experimental lung tumors. Again, the comparison between matched peri- versus intra-tumoral DC subpopulations allows addressing the influence of the tissue micro-environment on the observed changes. GSEA corroborates the findings obtained by surface expression analysis, pointing to the acquisition of TAM/M2-related properties by tumor-infiltrating CD11b<sup>+</sup> DCs. In addition, both GSEA and *in silico* prediction of transcription factor activity (ISMARA) indicate a loss of immunogenic/antigen-presenting function in TIDCs compared with peritumoral counterparts. GSEA reveals enrichment of TIDC transcriptomes with factors such as Arginase 1 and IL-10, already known to mediate active immune suppression in the LLC and other tumor models.<sup>27,31</sup> In line with this immunosuppressive signature, lung CD11b<sup>+</sup> TIDC also upregulate macrophage scavenger receptor 1 (MSR1) expression. MSR1 (SCARA1) was shown to impair tumor-antigen presentation by a mechanism

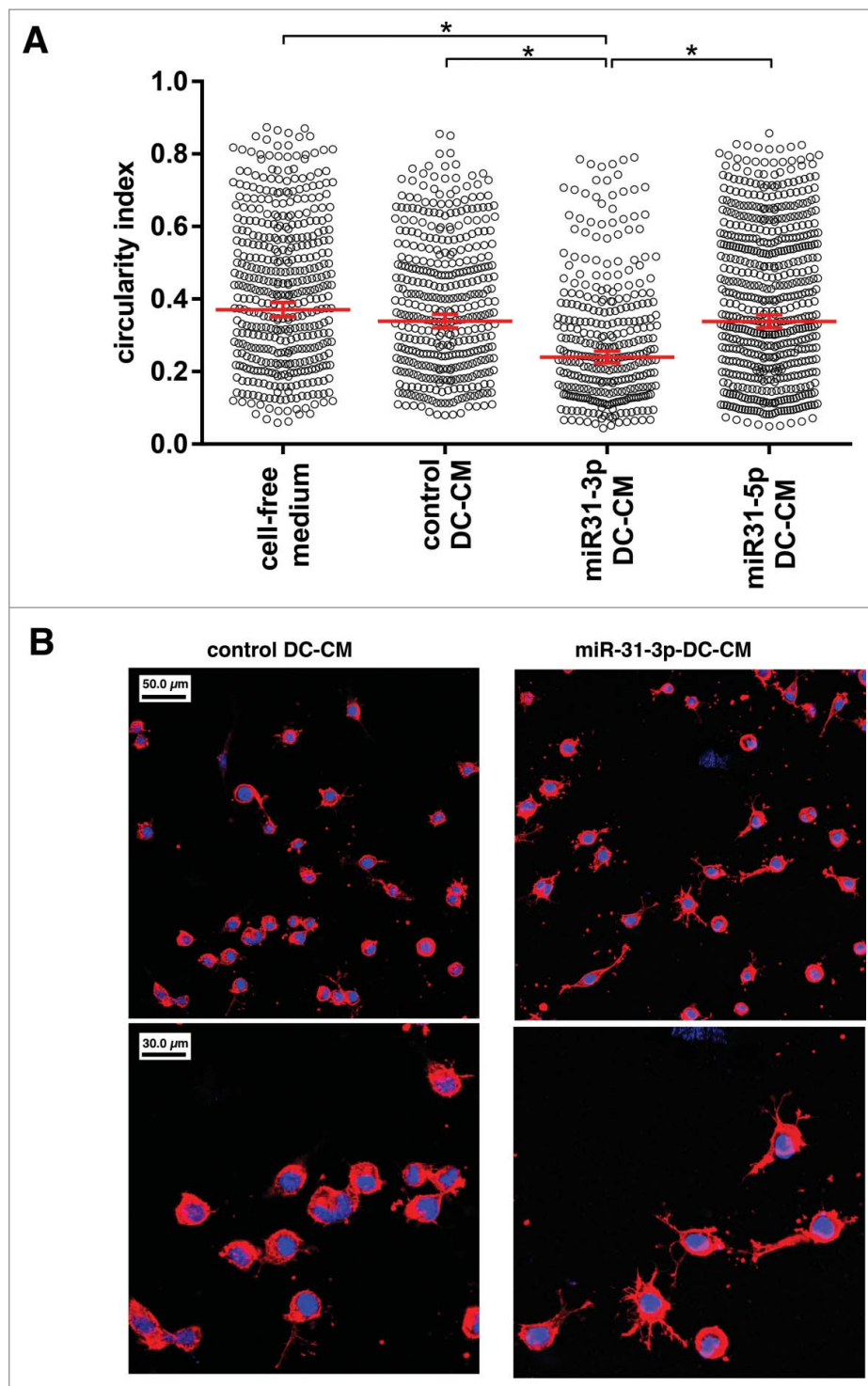


**Figure 8.** Conditioned medium from miR-31-3p overexpressing DCs induces pro-invasive lung cancer cell shape changes. (A) LLC cells seeded on a collagen type I membrane were exposed to cell-free culture medium or DC-conditioned medium (DC-CM) obtained from control- or miR-31-transfected BMDCs as indicated. Collagen matrices were fixed and stained for actin (red). Cell morphology parameters were computed using an automated image analysis algorithm. A drop in circularity index indicates cell elongation and/or the appearance of protrusions or filopodia. (B) Low- (upper row) and high-power (lower row) micrograph obtained by confocal imaging of LLC cells seeded on collagen type 1 matrices exposed to indicated DC-CM. DCs were generated from a pool of bone marrow cells from three mice to obtain sufficient conditioned medium.

involving increased uptake and accumulation of lipids in DCs.<sup>32</sup>

Another persistent pattern emerging from the lung TIDCs transcriptomes is the enrichment of gene expression and transcription factor activity reflecting *in vivo* exposure to hypoxia, a common physiological feature in the TME. Our studies show

that TIDC effectively co-localize with hypoxic areas within orthotopic LLC tumors. In DCs, hypoxia is known to induce large-scale alterations in gene expression.<sup>33-35</sup> The effects of hypoxia on TIDC could either be direct by promoting HIF-1 $\alpha$  accumulation, or indirect through the release of hypoxia-induced factors such as VEGF from surrounding cancer cells.

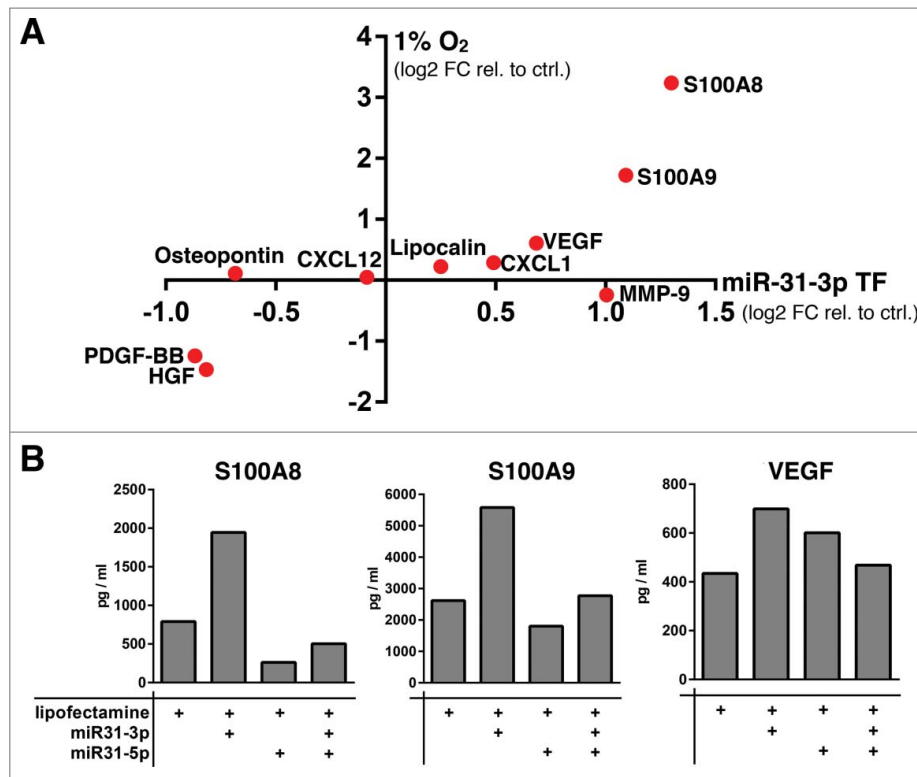


**Figure 9.** Hypoxic conditions and miR-31-3p overexpression trigger release of tumor-supporting soluble factors from myeloid DCs. DC-CMs obtained under the indicated culture conditions were analyzed for the presence of soluble factors using a multiplex analyte panel covering pro-metastatic and pro-angiogenic processes. (A) Data are expressed as log<sub>2</sub> of fold-changes relative to control culture condition or control transfection reagent respectively. (B) Quantitative measurement of soluble factors in DC-CM co-regulated by hypoxia and miR-31 overexpression alike, illustrating miR-31 transcript-specific effects. Data are obtained from proteomic analysis of supernatant pooled from separate BMDC cultures as described in Fig. 8.

Remarkably, the strongest upregulated genes in TIDCs in our study included MMP8, MMP9, and Cathepsin K, all three of which induced in pulmonary DCs when VEGF is overexpressed in the lung.<sup>36</sup> Also, in a LLC lung metastasis model, VEGF was shown to be a powerful inducer of MMP9 production in lung macrophages, thereby, promoting invasion of lung tissues by tumor cells.<sup>37</sup>

The mRNA expression data also supports a link between hypoxia exposure and the alteration of DC immunogenicity within the TME. For instance, TIDC show a significant upregulation of a prototypical hypoxia-related gene, 5'-nucleotidase (5'-NT, CD73).<sup>38</sup> As a membrane-bound enzyme, 5'-NT (CD73) catalyzes the breakdown of ATP in the extracellular space to generate adenosine, which is known to promote tolerance and immunosuppression through diverse autocrine and paracrine effects on DCs and/or T cells.<sup>39</sup> Moreover, PD-L1 upregulation, one of the most striking features of TIDCs in our model, was also shown to be induced by hypoxia in DCs, be it directly in a HIF-1 $\alpha$ -dependent manner or indirectly through the action of tumor-secreted VEGF.<sup>40,41</sup> Remarkably, *in silico* prediction of dominant transcription factor motifs indicates increased activity of two key TFs involved in endoplasmic reticulum stress response and cellular responses to hypoxia, i.e., XBP-1 and ATF-4.<sup>42</sup> This finding is also in line with a recent study, highlighting the role of ER-stress response in ovarian cancer infiltrating DCs.<sup>43</sup> In that particular study, increased activity of the ER-stress response TF XBP-1 leads to lipid accumulation in TIDCs, impaired antitumor immunity, and accelerated tumor progression. Collectively, these and our results

warrant investigations on the potential therapeutic impact of ER-stress modulation in the myeloid compartment of the lung cancer stroma.

Our study is the first to perform genome-wide mRNA and miRNA expression analysis in parallel on matched *ex vivo* purified peritumoral and TIDCs. Using the same preclinical lung cancer model, we previously demonstrated that a subset of DCs transporting lung tumor antigens to the draining lymph nodes expresses a set of miRNAs that sabotages the capacity to induce T helper 1 responses.<sup>44</sup> Here, we report on the microRNome of the lung tumor resident DC population and reveal the forceful upregulation of miR-31 transcripts when compared with peritumoral DC counterparts. In lung cancer, miR-31 is associated with poor survival, lymph node metastasis, resistance to chemotherapy and perturbation of cell cycle by targeting DNA mismatch repair genes.<sup>45-49</sup> MiR-31 expression is closely associated with hypoxia-responsive pathways, as it targets FIH to de-repress HIF-1 $\alpha$  activity, thus, boosting transcription of hypoxia-responsive genes (e.g., pro-angiogenic factors). Although intratumoral overexpression of miR-31 relative to matched non-cancerous tissue has been described in human and animal models of lung cancer<sup>50</sup> upregulation of this oncomir within a critical cell of the immune compartment of a tumor has not been documented before. Our finding supports a concept elegantly put forward in a study by Hanahan et al., in which miRNA signatures associated with different stages of tumor progression were shown to originate from the leukocytic infiltrate, rather than from the cancer cells themselves.<sup>51</sup> As we found that hypoxia is by itself a major driver of miR-31

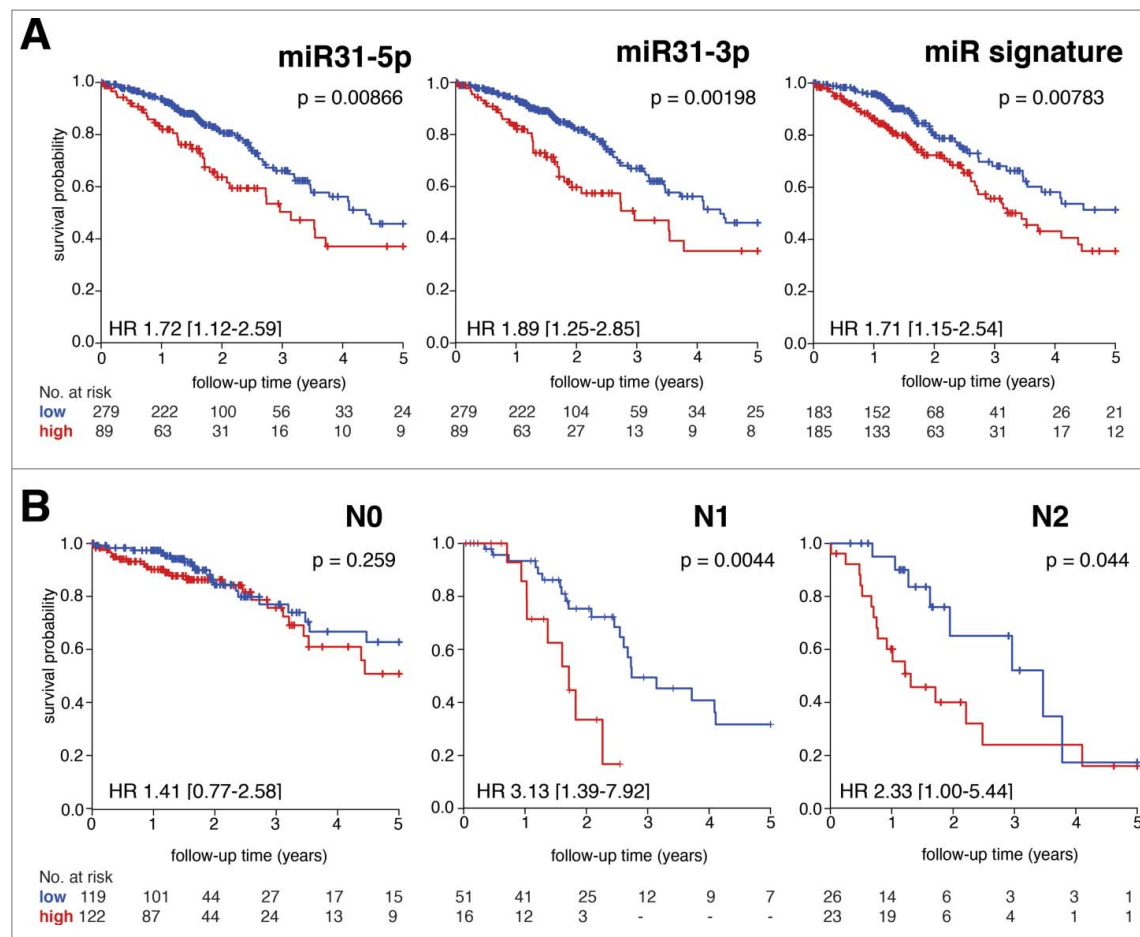


**Figure 10.** Prognostic impact of miR-31 expression and tumor-infiltrating DC-derived miRNA signature in non-squamous non-small cell lung cancer ( $n = 368$  patients). (A) TCGA clinical dataset analyzed using Cox-proportional hazard regression as well as Kaplan–Meier statistics, all TNM stages. For miR-31-5p and miR-31-3p, the highest expression quartile segregated patients with significantly worse overall survival. For the miRNA signature, patients with a ranked sum above the mean (strong signature) demonstrate a worse outcome. (B) Differential impact of TIDC signature strength according to lymph node invasion stage. Patients were divided into two groups based on mean (N1/N2) or highest rank sum quartile (N0).

expression in CD11b<sup>+</sup> DCs, we propose that reprogramming of miRNA expression in myelomonocytic cells contributes to the tumor-supporting effects of hypoxia. Indeed, we observed that conditioned medium of DCs overexpressing miR-31-3p could

induce lung cancer cell shape changes indicative of increased invasive behavior. In particular, the observed appearance of filopodia-like protrusions was shown by Weinberg et al. to be a strong indicator of metastatic potential.<sup>23</sup> Remarkably, we

**Table 1.** Kaplan–Meier and Cox-proportional hazards statistics derived from non-squamous non-small cell lung cancer survival data (The Cancer Genome Atlas, <https://tcga-data.nci.nih.gov>), as a function of miR-31 and TIDC expression strength.

	Median OS (years)	5-y survival rate	HR for death [95% CI]	Cox PH $p$ -value
miR-31-5p expression (cut-off: upper quartile of normalized expression)				
Low	4.4	45.8%	1.72 [1.12–2.59]	0.00972
High	3.1	37.1%		
miR-31-3p expression (cut-off: upper quartile of normalized expression)				
Low	4.4	46.1%	1.89 [1.25–2.85]	0.00234
High	3.0	35.3%		
TIDC miR signature strength				
Low	N.R.	51.3%	1.71 [1.15–2.54]	0.00859
High	3.4	35.5%		
N0 (cut-off: upper quartile of rank-sum)				
Low	N.R.	62.8%	1.41 [0.77–2.58]	0.547
High	N.R.	50.8%		
N1 (cut-off: median of rank-sum)				
Low	2.74	31.7%	3.13 [1.39–7.92]	0.0247
High	1.72	16.7%		
N2 (cut-off: median of rank-sum)				
Low	3.47	17.4%	2.33 [1.00–5.44]	0.0991
High	1.31	16.0%		

HR = hazard ratio, CI = confidence interval, PH = proportional hazard, N.R. = not reached.

found that DCs specifically overexpressing miR-31-3p or exposed to hypoxia released high amounts of the tumor-supporting factors S100A8, S100A9. An earlier report by Hiratsuka and coworkers showed that tumor-derived VEGF is a major stimulus for S100A8 secretion by CD11b<sup>+</sup> leukocytes.<sup>52</sup> In these studies, the strong chemotactic activity of S100A8 emerged as a common pathway critical for the recruitment of both pro-tumorigenic CD11b<sup>+</sup> leukocytes as well as lung cancer cells toward intrapulmonary niches. Moreover, S100A8 was shown to induce foci of vascular hyperpermeability within the lungs, thereby, creating a milieu conducive for intrapulmonary tumor establishment.<sup>53</sup> In a recent study, S100A8/A9 proteins secreted by tumor-associated DCs was implicated in breast cancer chemoresistance.<sup>54</sup> Moreover S100A9 was shown to skew haematopoietic stem cell differentiation away from DCs, favoring expansion of immature myeloid cells with T-cell suppressive activity.<sup>55</sup> Accordingly, advanced lung cancer patients show an increase in S100A9-expressing inflammatory monocytes that suppress T-cell responses and are associated with worse prognosis.<sup>56</sup> S100-protein release may only partially contribute to the pro-tumoral effects of miR-31 upregulation in myeloid DCs. Future *in vivo* studies, either using conditional ablation of the miR-31 gene in monocytes or specific DC subsets or administration of DC-targeted anti-miRs, will provide additional mechanistic evidence for the importance of DC-derived miR-31 in promoting lung tumor progression.

Accumulating evidence indicates that the status of DCs in the lung TME can impact on patient outcome in lung cancer (see *Introduction* section for references). Hence, we explored whether the miRNA signature extracted from “corrupt” tumor-associated DCs could have a negative effect on prognosis in this disease. Not only were we able to confirm the negative prognostic impact of miR-31 in lung cancer as suggested by previous reports, but also we could observe that the strength of the TIDC-derived miRNA-signature as a whole negatively affects overall survival in this disease. Over a follow-up period of 5 y, patients with high signature strength had a 70% relative increase in risk of death, with a median overall survival of 3.4 y, which is worse than expected for this group of resectable (i.e., “early stage”) lung cancer cases. In patients with low signature strength, median overall survival was not reached over the 5-y horizon. Remarkably, the TIDC-derived miRNA signature had a dramatic impact on prognosis once nodal invasion was present. For resected lung cancer with N1 status (first lymph node station invaded by carcinoma), there was a 3-fold risk for death in the group with high TIDC signature strength, with a 5-y survival rate comparable to the more advanced N2 (stage III) patients. We believe this observation might reflect a clinically relevant skewing of DC biology from an immunogenic to a metastasis-supporting stromal cell, and warrants a prospective validation of this miRNA signature in non-small cell lung cancer. Also, the fact that the prognostic effects were only observed in adenocarcinoma and not in squamous cell lung cancer should draw our attention to differences in immune contexture among lung cancer histological subtypes.

In summary, although our study confirms the generally accepted view of tumor-induced DC “corruption,” we also provide evidence for a unique reverse effect in which a DC-intrinsic miRNA signature links exposure to intratumoral hypoxia

with the acquisition of tumor-supporting properties. It is now clear that modulating the immune balance in the TME is establishing itself as a remarkably efficacious therapeutic strategy against several solid tumors, including lung cancer.<sup>57</sup> As DCs are central orchestrators of immune responses, we believe that efforts to reverse the corruption of these cells in the tumor environment may ultimately enrich the growing arsenal of successful cancer immunotherapeutics.

## Materials and methods

### Cell culture and transfection experiments

The murine Lewis lung carcinoma (LLC-A) cell line on C57Bl/6 background was provided by M. Bracke (Ghent University, Belgium) and maintained in DMEM (Gibco, Invitrogen), supplemented with 10% fetal bovine serum (Sigma-Aldrich) and 1000 U/mL penicillin/streptomycin (Gibco, Invitrogen). Bone marrow derived DCs were generated as described previously.<sup>58</sup> Briefly, murine bone marrow cell suspensions were cultured for a total of 8 d in RPMI 1640 supplemented with 5% iFBS, L-Glutamine, gentamycin (2.8 mL),  $5 \times 10^{-5}$  M  $\beta$ -mercaptoethanol (Life Technologies), and 20 ng/mL mouse recombinant GM-CSF (gift from K. Thielemans, Free University of Brussels, Belgium). Fresh medium with cytokines was added on day 3 and on day 6. For hypoxia experiments, day 6 DCs were placed under low environmental oxygen conditions (1% O<sub>2</sub>) for 48 h. Twelve to sixteen hours before harvest, the cells were stimulated with 100 ng/mL LPS (Invivogen). In transfection experiments, day 6 BMDCs were seeded in 24-well ultra-low attachment plates (Corning, Inc.). Thereafter, 100 nM of a mimic or inhibitor of miR-31-3p, miR-31-5p, or control mimic/inhibitor (all from Ambion) was transfected using 1  $\mu$ L RNAiMax lipofectamine (Invitrogen). Cy3-labeled control anti-miRNA (Ambion) was used to determine transfection efficiency.

### Orthotopic lung tumor model and *in vivo* imaging

Seven- to eight-week-old female wild-type C57BL/6 mice (Harlan) were housed at Ghent University (Ghent, Belgium) animal facility in individually ventilated cages. The Animal Ethics Committee of Ghent University approved all *in vivo* manipulations. Mice were anesthetized with ketamine (65 mg/kg, Ceva) and xylazine (6.5 mg/kg, Verdifarm). Sterile saline solution (70  $\mu$ L) containing  $1.5 \times 10^6$  LLC or luciferase expressing LLC cells was transferred into the airways using a non-invasive supralaryngeal instillation technique. For cross-sectional endpoint experiments, mice were sacrificed and analyzed at 28–32 d post-implantation. For survival experiments, animals were euthanized at  $\geq 15\%$  weight loss or at signs of illness (as per Canadian Council on Animal Care guidelines).

### Flow cytometry and cell sorting

Lung tumors and peritumoral lung tissues were harvested from LLC bearing mice. Cell suspensions were prepared as described before.<sup>44</sup> Single-cell suspensions were incubated with anti-mouse monoclonal antibody combinations for 30 min at 4 °C

in the presence of Fc $\gamma$  III/II receptor antibody (clone 2.4G2) to block non-specific binding. Antibodies used for staining are described in Table S1. Samples were acquired on an LSRII and LSRFortessa cytometer (BD Biosciences) and data were analyzed using FlowJo software (Tree Star, Inc.). Surface marker data were expressed as relative mean fluorescence intensity calculated as the ratio of geometrical mean fluorescence intensity (geo-MFI) of the specific staining antibody over geo-MFI of matched isotype control. For fluorescence-activated cell sorting (FACS) experiments, CD3<sup>-</sup>/CD19<sup>-</sup>/low auto-fluorescent/CD45<sup>+</sup>/MHCII<sup>+</sup>/CD11c<sup>+</sup>/CD11b<sup>+</sup> DCs were sorted from lungs or tumor from tumor-bearing and control mice on a FACS Aria II and III cytometer (BD Biosciences). Sort purity was consistently more than 90%.

### Gene expression analysis of FAC-sorted DCs

For mouse gene expression analysis of tumor-exposed DCs, DCs were FAC-sorted from tumor and peritumoral lung tissues from tumor-bearing mice. Total RNA was extracted from DCs using the miRNeasy kit (Qiagen) according to manufacturer's instruction. Quality checks were performed on an Experion automated electrophoresis system (RQI). The Affymetrix mouse gene ST1.0 array was used with 100 ng total RNA as input. Analysis of the microarray data was performed in the R programming environment, in conjunction with the packages developed within the Bioconductor project (<http://www.bioconductor.org>). The analysis was based on the RMA expression levels of the probe sets, as obtained with the xps-package. Differential expression was assessed with the limma-package via Smyth's moderated *t*-statistic, taking into account that the data were paired. Genes were selected by means of the criterion used in the MAQC-I study,<sup>13</sup> based on *p*-value < 0.001, further constrained to genes with an absolute log<sub>2</sub>-ratio > 1. Data have been deposited in Gene Expression Omnibus under accession number GSE85044 and can be viewed at <http://www.ncbi.nlm.nih.gov/geo/query/acc.cgi?acc=GSE85044>.

### In silico functional transcriptome analysis

Further *in silico* exploration of differential gene expression was performed using Gene Set Enrichment Analysis,<sup>59,60</sup> using comprehensive, curated gene lists for biological processes relevant in this model (see Table S1). Prediction of transcription factor activity driving the observed differential gene expression was performed using Integrated System for Motif Activity Response Analysis (ISMARA<sup>17</sup>), which is a web-based algorithm that infers a regulator's activity by the behavior of its targets (without relying directly on the expression levels of a transcription factor).

### MiRNA expression analysis of FAC-sorted DCs and in silico target gene prediction

For miRNA expression analysis of tumor-exposed DCs, the same RNA as for the mouse exon array was used in high throughput RT-qPCR based TaqMan miRNA assays (Applied Biosystems) according to our previously described method.<sup>44,61</sup> MiRNA expression data was normalized using the global mean

expression of all expressed miRNAs (based on a Cq-value cut-off of 32 cycles).<sup>62</sup> After normalization, missing miRNA expression data were imputed using the lowest expression for the respective miRNA. Differentially expressed miRNAs were selected using a rank product test (percentage false positives < 5). Hierarchical clustering was performed using R Bioconductor software (method Ward, distance Manhattan). Expression of murine miR-31-3p and miR-31-5p expression was quantified by RT-qPCR (TaqMan microRNA assay, Applied Biosystems) with snoRNA202 and U6 as endogenous control RNA. Fold changes were calculated using the  $\Delta\Delta$ Ct method.

### Tumor histology and immunofluorescence staining

Lungs of tumor-bearing mice were inflated with 1:1 solution of OCT/PBS; in some experiments, animals were previously injected intravenously with 60 mg/kg Hypoxyprobe (Hypoxyprobe Inc., Burlington). Frozen sections (6- $\mu$ m thick) were fixed in 4% formaldehyde for 10 min and stained with hematoxylin and eosin. In some experiments sections were blocked for 30 min in Blocking Reagent (Roche) containing 10% normal rabbit serum. After washing, slides were stained for 1 h at room temperature with monoclonal antibodies against CD11c (efluor660, clone N418, eBioscience), and pimonidazole (FITC, Hypoxyprobe Inc., Burlington). After washing, slides were incubated 1 h with alexa fluor 488-labeled anti-fluorescein antibody (Life Technologies) and DAPI nuclear counterstain. Microscopic examinations were performed on a LSM710 confocal laser scanning microscope (Carl Zeiss, Inc.) and images were analyzed using Imaris 5.0 software (Bitplane).

### Collagen invasion assay

Type I collagen solution was produced as described previously<sup>63</sup> and dispensed into six-well plates for gelification in a humidified atmosphere of 10% CO<sub>2</sub> in air at 37 °C for at least 1 h. 1  $\times$  10E6 LLC cells were seeded in each well on top of the gel, and the plates were placed for 24 h in a humidified CO<sub>2</sub> incubator. Gels were then fixed in a 3% formalin solution and stained with phalloidin-TexasRed (Sigma) with DAPI nuclear counterstain. Images of the gels were acquired on confocal laser scanning microscope at 20 $\times$  magnification. Images were subsequently processed in ImageJ, using algorithms for cell contour detection and calculation of the circularity shape index. The shape index is a continuous variable between 0 and 1 and indicates deviation from a perfect circular contour: a shape index of one indicates perfect cellular sphericity, with lower values reflecting cell elongation and/or the presence of cytoplasmic protrusions. Approximately 50–100 cells were analyzed per image, and five images were acquired per experimental condition.

### Proteomic analysis

Conditioned media from control versus miRNA-transfected bone marrow-derived DCs were analyzed using a Luminex biomarker screening assay (R&D Systems), according to the manufacturer's instructions. The assay was custom-designed for the simultaneous measurement of 17 analytes with pro-angiogenic and/or pro-metastatic functions (KC/CXCL-1, Dkk-1, G-CSF,



HGF, Lipocalin-2/N-GAL, Osteopontin, Periostin/OSF-2, S100A8, S100A9, SDF-1 $\alpha$ /CXCL12, EMMPRIN/CD147, GDF-15, Leptin, MMP-9, PDGF-BB, Resistin, and VEGF).

### TCGA data mining

The clinical expression analysis is based on genome-wide Illumina miRNA-sequencing data from 521 patient lung adenocarcinoma and squamous cell carcinoma tumor samples, retrieved from TCGA. Bam files were converted to fastq and remapped using Bowtie (v.1.0.0). Mapped reads were annotated based on miRBase 20. The expression levels of the selected miRNAs for all patients were combined with clinical data available at TCGA Data Portal [<https://tcga-data.nci.nih.gov/tcga/>]. The effect of survival was examined with the Cox proportional hazard regression model. The Wald test was used to test significance ( $p$ -value less than 0.05). Patient survival curves were estimated by the Kaplan–Meier method using the survival package (2.38–3) in R (3.2.2). Patients were categorized into groups with high and low expression for both miR-31 arms, based on the 75% quartile,  $p$ -values were calculated using the log-rank test. For the signature, a rank-sum was calculated and patients were divided into two groups based on the median. We calculated the hazard ratio, median overall survival and 5 y survival rate based on the cox proportional hazard regression model.

### Statistical analysis

For all experiments except abovementioned genomic and survival analyses, differences between groups were analyzed using the non-parametric Mann–Whitney  $U$  or Kruskal–Wallis test with post-hoc Dunn's test. Differences were considered statistically significant if  $p$ -value < 0.05 ( $*p < 0.05$ ,  $**p < 0.01$ ,  $***p < 0.001$ ) with error bars representing SEM. Data were analyzed using GraphPad Prism v6.0 (GraphPad Software, Inc.).

### Disclosure of potential conflicts of interest

No potential conflicts of interest were disclosed.

### Acknowledgments

Affymetrix array analyses were performed at the VIB Nucleomics Core ([www.nucleomics.be/](http://www.nucleomics.be/)). We thank the animal caretakers of Ghent University. The authors have no conflicting financial interests to declare in relation to this report.

### Funding

LP is supported by IWT grant SB/083359 and IUAP VII-project grant 120C07912W. EB is supported by Ghent University Concerted Research Initiative BOF24/GOA/027. This project is funded by FWO Research Project grant G.A015.11 and the Foundation Against Cancer grant STK 2010–182. K. Vermaelen is supported by a FWO Senior Clinical Investigator award.

### ORCID

Celine Everaert  <http://orcid.org/0000-0001-7772-4259>  
Melissa Dullaers  <http://orcid.org/0000-0003-0223-230X>  
Jo Vandesompele  <http://orcid.org/0000-0001-6274-0184>

### References

- Kastenmüller W, Kastenmüller K, Kurts C, Seder RA. Dendritic cell-targeted vaccines—hope or hype? *Nat Rev Immunol* 2014; 14:705–11; PMID:25190285; <http://dx.doi.org/10.1038/nri3727>
- Palucka K, Banchereau J. Cancer immunotherapy via dendritic cells. *Nat Rev Cancer* 2012; 12:265–77; PMID:22437871; <http://dx.doi.org/10.1038/nrc3258>
- Koebel CM, Vermi W, Swann JB, Zerafa N, Rodig SJ, Old LJ, Smyth MJ, Schreiber RD. Adaptive immunity maintains occult cancer in an equilibrium state. *Nature* 2007; 450:903–7; PMID:18026089; <http://dx.doi.org/10.1038/nature06309>
- Remark R, Becker C, Gomez JE, Damotte D, Dieu-Nosjean MC, Sautes-Fridman C, Fridman WH, Powell CA, Altorki NK, Merad M et al. The non-small cell lung cancer immune contexture. A major determinant of tumor characteristics and patient outcome. *Am J Respir Critical Care Med* 2015; 191:377–90; PMID:25369536; <http://dx.doi.org/10.1164/rccm.201409-1671PP>
- Inoshima N, Nakanishi Y, Minami T, Izumi M, Takayama K, Yoshino I, Hara N. The influence of dendritic cell infiltration and vascular endothelial growth factor expression on the prognosis of non-small cell lung cancer. *Clin Cancer Res* 2002; 8:3480–6; PMID:12429638
- Goc J, Germain C, Vo-Bourgeois TK, Lupo A, Klein C, Knockaert S, de Chaisemartin L, Ouakrim H, Becht E, Alifano M et al. Dendritic cells in tumor-associated tertiary lymphoid structures signal a Th1 cytotoxic immune contexture and license the positive prognostic value of infiltrating CD8+ T cells. *Cancer Res* 2014; 74:705–15; PMID:24366885; <http://dx.doi.org/10.1158/0008-5472.CAN-13-1342>
- Zong J, Keskinov AA, Shurin GV, Shurin MR. Tumor-derived factors modulating dendritic cell function. *Cancer Immunol Immunother* 2016; 65:821–33; PMID:26984847; <http://dx.doi.org/10.1007/s00262-016-1820-y>
- Perrot I, Blanchard D, Freymond N, Isaac S, Guibert B, Pacheco Y, Lebecque S. Dendritic cells infiltrating human non-small cell lung cancer are blocked at immature stage. *J Immunol* 2007; 178:2763–9; PMID:17312119; <http://dx.doi.org/10.4049/jimmunol.178.5.2763>
- Norian LA, Rodriguez PC, O'Mara LA, Zabaleta J, Ochoa AC, Cella M, Allen PM. Tumor-infiltrating regulatory dendritic cells inhibit CD8+ T cell function via L-arginine metabolism. *Cancer Res* 2009; 69:3086–94; PMID:19293186; <http://dx.doi.org/10.1158/0008-5472.CAN-08-2826>
- Zheng X, Koropatnick J, Chen D, Velenosi T, Ling H, Zhang X, Jiang N, Navarro B, Ichim TE, Urquhart B et al. Silencing IDO in dendritic cells: a novel approach to enhance cancer immunotherapy in a murine breast cancer model. *Int J Cancer* 2013; 132:967–77; PMID:22870862; <http://dx.doi.org/10.1002/ijc.27710>
- Gabrilovich DI, Ostrand-Rosenberg S, Bronte V. Coordinated regulation of myeloid cells by tumours. *Nat Rev Immunol* 2012; 12:253–68; PMID:22437938; <http://dx.doi.org/10.1038/nri3175>
- Plantinga M, Guillems M, Vanheerswynghels M, Deswarte K, Branco-Madeira F, Toussaint W, Vanhoutte L, Neyt K, Killeen N, Malissen B et al. Conventional and monocyte-derived CD11b(+) dendritic cells initiate and maintain T helper 2 cell-mediated immunity to house dust mite allergen. *Immunity* 2013; 38:322–35; PMID:23352232; <http://dx.doi.org/10.1016/j.immuni.2012.10.016>
- Shi L, Reid LH, Jones WD, Shippy R, Warrington JA, Baker SC, Collins PJ, de Longueville F, Kawasaki ES, Lee KY et al. The Micro-Array Quality Control (MAQC) project shows inter- and intraplatform reproducibility of gene expression measurements. *Nat Biotechnol* 2006; 24:1151–61; PMID:16964229; <http://dx.doi.org/10.1038/nbt1239>
- Shen XZ, Okwan-Duodu D, Blackwell WL, Ong FS, Janjulia T, Bernstein EA, Fuchs S, Alkan S, Bernstein KE. Myeloid expression of angiotensin-converting enzyme facilitates myeloid maturation and inhibits the development of myeloid-derived suppressor cells. *Lab Invest* 2014; 94:536–44; PMID:24614194; <http://dx.doi.org/10.1038/labinvest.2014.41>
- Deng J, Fujimoto J, Ye XF, Men TY, Van Pelt CS, Chen YL, Lin XF, Kadara H, Tao Q, Lotan D et al. Knockout of the tumor suppressor gene Gprc5a in mice leads to NF-kappaB activation in airway epithelium and promotes lung inflammation and tumorigenesis. *Cancer*

- Prevent Res 2010; 3:424-37; PMID:20354164; <http://dx.doi.org/10.1158/1940-6207.CAPR-10-0032>
16. Subramanian A, Tamayo P, Mootha VK, Mukherjee S, Ebert BL, Gillette MA, Paulovich A, Pomeroy SL, Golub TR, Lander ES et al. Gene set enrichment analysis: a knowledge-based approach for interpreting genome-wide expression profiles. *Proc Natl Acad Sci USA* 2005; 102:15545-50; PMID:16199517; <http://dx.doi.org/10.1073/pnas.0506580102>
  17. Balwiercz PJ, Pachkov M, Arnold P, Gruber AJ, Zavolan M, van Nimwegen E. ISMARA: automated modeling of genomic signals as a democracy of regulatory motifs. *Genome Res* 2014; 24:869-84; PMID:24515121; <http://dx.doi.org/10.1101/gr.169508.113>
  18. Belladonna ML, Renaud JC, Bianchi R, Vacca C, Fallarino F, Orabona C, Fioretti MC, Grohmann U, Puccetti P. IL-23 and IL-12 have overlapping, but distinct, effects on murine dendritic cells. *J Immunol* 2002; 168:5448-54; PMID:12023338; <http://dx.doi.org/10.4049/jimmunol.168.11.5448>
  19. Fukao T, Frucht DM, Yap G, Gadina M, O'Shea JJ, Koyasu S. Inducible expression of Stat4 in dendritic cells and macrophages and its critical role in innate and adaptive immune responses. *J Immunol* 2001; 166:4446-55; PMID:11254700; <http://dx.doi.org/10.4049/jimmunol.166.7.4446>
  20. Wu L, Yan C, Czader M, Foreman O, Blum JS, Kapur R, Du H. Inhibition of PPARgamma in myeloid-lineage cells induces systemic inflammation, immunosuppression, and tumorigenesis. *Blood* 2012; 119:115-26; PMID:22053106; <http://dx.doi.org/10.1182/blood-2011-06-363093>
  21. Xu Y, Zhan Y, Lew AM, Naik SH, Kershaw MH. Differential development of murine dendritic cells by GM-CSF versus Flt3 ligand has implications for inflammation and trafficking. *J Immunol* 2007; 179:7577-84; PMID:18025203; <http://dx.doi.org/10.4049/jimmunol.179.11.7577>
  22. Helft J, Bottcher J, Chakravarty P, Zelenay S, Huotari J, Schraml BU, Goubau D, Reis e Sousa C. GM-CSF mouse bone marrow cultures comprise a heterogeneous population of CD11c(+)MHCII(+) macrophages and dendritic cells. *Immunity* 2015; 42:1197-211; PMID:26084029; <http://dx.doi.org/10.1016/j.immuni.2015.05.018>
  23. Shibue T, Brooks MW, Inan MF, Reinhardt F, Weinberg RA. The outgrowth of micrometastases is enabled by the formation of filopodium-like protrusions. *Cancer Disco* 2012; 2:706-21; PMID:22609699; <http://dx.doi.org/10.1158/2159-8290.CD-11-0239>
  24. Franklin RA, Liao W, Sarkar A, Kim MV, Bivona MR, Liu K, Pamer EG, Li MO. The cellular and molecular origin of tumor-associated macrophages. *Science* 2014; 344:921-5; PMID:24812208; <http://dx.doi.org/10.1126/science.1252510>
  25. Broz ML, Binnewies M, Boldajipour B, Nelson AE, Pollack JL, Erle DJ, Barczak A, Rosenblum MD, Daud A, Barber DL et al. Dissecting the tumor myeloid compartment reveals rare activating antigen-presenting cells critical for T cell immunity. *Cancer Cell* 2014; 26:638-52; PMID:25446897; <http://dx.doi.org/10.1016/j.ccell.2014.09.007>
  26. Lohela M, Casbon AJ, Olow A, Bonham L, Branstetter D, Weng N, Smith J, Werb Z. Intravital imaging reveals distinct responses of depleting dynamic tumor-associated macrophage and dendritic cell subpopulations. *Proc Natl Acad Sci USA* 2014; 111:E5086-95; PMID:25385645; <http://dx.doi.org/10.1073/pnas.1419899111>
  27. Diao J, Mikhailova A, Tang M, Gu H, Zhao J, Cattral MS. Immunostimulatory conventional dendritic cells evolve into regulatory macrophage-like cells. *Blood* 2012; 119:4919-27; PMID:22490680; <http://dx.doi.org/10.1182/blood-2011-11-392894>
  28. Peng Y, Latchman Y, Elkon KB. Ly6C(low) monocytes differentiate into dendritic cells and cross-tolerize T cells through PDL-1. *J Immunol* 2009; 182:2777-85; PMID:19234172; <http://dx.doi.org/10.4049/jimmunol.0803172>
  29. Salmon H, Idoyaga J, Rahman A, Leboeuf M, Remark R, Jordan S, Casanova-Acebes M, Khudoynazarova M, Agudo J, Tung N et al. Expansion and activation of CD103(+) dendritic cell progenitors at the tumor site enhances tumor responses to therapeutic PD-L1 and BRAF inhibition. *Immunity* 2016; 44:924-38; PMID:27096321; <http://dx.doi.org/10.1016/j.immuni.2016.03.012>
  30. Fehrenbacher L, Spira A, Ballinger M, Kowanetz M, Vansteenkiste J, Mazieres J, Park K, Smith D, Artal-Cortes A, Lewanski C et al. Atezolizumab versus docetaxel for patients with previously treated non-small-cell lung cancer (POPLAR): a multicentre, open-label, phase 2 randomised controlled trial. *Lancet* 2016; 387:1837-46; PMID:26970723; [http://dx.doi.org/10.1016/S0140-6736\(16\)00587-0](http://dx.doi.org/10.1016/S0140-6736(16)00587-0)
  31. Liu Q, Zhang C, Sun A, Zheng Y, Wang L, Cao X. Tumor-educated CD11bhighIalow regulatory dendritic cells suppress T cell response through arginase I. *J Immunol* 2009; 182:6207-16; PMID:19414774; <http://dx.doi.org/10.4049/jimmunol.0803926>
  32. Herber DL, Cao W, Nefedova Y, Novitskiy SV, Nagaraj S, Tyurin VA, Corzo A, Cho HI, Celis E, Lennox B et al. Lipid accumulation and dendritic cell dysfunction in cancer. *Nature Med* 2010; 16:880-6; PMID:20622859; <http://dx.doi.org/10.1038/nm.2172>
  33. Blengio F, Raggi F, Pierobon D, Cappello P, Eva A, Giovarelli M, Varesio L, Bosco MC. The hypoxic environment reprograms the cytokine/chemokine expression profile of human mature dendritic cells. *Immunobiology* 2013; 218:76-89; PMID:22465745; <http://dx.doi.org/10.1016/j.imbio.2012.02.002>
  34. Bosco MC, Pierobon D, Blengio F, Raggi F, Vanni C, Gattorno M, Eva A, Novelli F, Cappello P, Giovarelli M et al. Hypoxia modulates the gene expression profile of immunoregulatory receptors in human mature dendritic cells: identification of TREM-1 as a novel hypoxic marker in vitro and in vivo. *Blood* 2011; 117:2625-39; PMID:21148811; <http://dx.doi.org/10.1182/blood-2010-06-292136>
  35. Pierobon D, Bosco MC, Blengio F, Raggi F, Eva A, Filippi M, Musso T, Novelli F, Cappello P, Varesio L et al. Chronic hypoxia reprograms human immature dendritic cells by inducing a proinflammatory phenotype and TREM-1 expression. *Eur J Immunol* 2013; 43:949-66; PMID:23436478; <http://dx.doi.org/10.1002/eji.201242709>
  36. Chapoval SP, Lee CG, Tang C, Keegan AD, Cohn L, Bottomly K, Elias JA. Lung vascular endothelial growth factor expression induces local myeloid dendritic cell activation. *Clinical Immunol* 2009; 132:371-84; PMID:19553159; <http://dx.doi.org/10.1016/j.clim.2009.05.016>
  37. Hiratsuka S, Nakamura K, Iwai S, Murakami M, Itoh T, Kijima H, Shipley JM, Senior RM, Shibuya M. MMP9 induction by vascular endothelial growth factor receptor-1 is involved in lung-specific metastasis. *Cancer Cell* 2002; 2:289-300; PMID:12398893; [http://dx.doi.org/10.1016/S1535-6108\(02\)00153-8](http://dx.doi.org/10.1016/S1535-6108(02)00153-8)
  38. Synnestvedt K, Furuta GT, Comerford KM, Louis N, Karhausen J, Eltzschig HK, Hansen KR, Thompson LF, Colgan SP. Ecto-5'-nucleotidase (CD73) regulation by hypoxia-inducible factor-1 mediates permeability changes in intestinal epithelia. *J Clin Invest* 2002; 110:993-1002; PMID:12370277; <http://dx.doi.org/10.1172/JCI0215337>
  39. Challier J, Bruniquel D, Sewell AK, Laugel B. Adenosine and cAMP signalling skew human dendritic cell differentiation towards a tolerogenic phenotype with defective CD8(+) T-cell priming capacity. *Immunology* 2013; 138:402-10; PMID:23278551; <http://dx.doi.org/10.1111/imm.12053>
  40. Curiel TJ, Wei S, Dong H, Alvarez X, Cheng P, Mottram P, Krzysiek R, Knutson KL, Daniel B, Zimmermann MC et al. Blockade of B7-H1 improves myeloid dendritic cell-mediated antitumor immunity. *Nat Med* 2003; 9:562-7; PMID:12704383; <http://dx.doi.org/10.1038/nm863>
  41. Noman MZ, Desantis G, Janji B, Hasmim M, Karray S, Dessen P, Bronte V, Chouaib S. PD-L1 is a novel direct target of HIF-1alpha, and its blockade under hypoxia enhanced MDSC-mediated T cell activation. *J Exp Med* 2014; 211:781-90; PMID:24778419; <http://dx.doi.org/10.1084/jem.20131916>
  42. Chen X, Iliopoulos D, Zhang Q, Tang Q, Greenblatt MB, HatziaPOSTOLOU M, Lim E, Tam WL, Ni M, Chen Y et al. XBPI promotes triple-negative breast cancer by controlling the HIF1alpha pathway. *Nature* 2014; 508:103-7; PMID:24670641; <http://dx.doi.org/10.1038/nature13119>
  43. Cubillos-Ruiz JR, Silberman PC, Rutkowski MR, Chopra S, Perales-Puchalt A, Song M, Zhang S, Bettigole SE, Gupta D, Holcomb K et al. ER stress sensor XBPI controls anti-tumor immunity by disrupting dendritic cell homeostasis. *Cell* 2015; 161:1527-38; PMID:26073941; <http://dx.doi.org/10.1016/j.cell.2015.05.025>
  44. Pyfferoen L, Mestdagh P, Vergote K, De Cabooter N, Vandesompele J, Lambrecht BN, Vermaelen KY. Lung tumours reprogram pulmonary dendritic cell immunogenicity at the microRNA level. *Int J Cancer* 2014; 135:2868-77; PMID:24789737; <http://dx.doi.org/10.1002/ijc.28945>

45. Wang S, Hu J, Zhang D, Li J, Fei Q, Sun Y. Prognostic role of microRNA-31 in various cancers: a meta-analysis. *Tumour Biol* 2014; 35:11639-45; PMID:25139099; <http://dx.doi.org/10.1007/s13277-014-2492-x>
46. Meng W, Ye Z, Cui R, Perry J, Dedousi-Huebner V, Huebner A, Wang Y, Li B, Volinia S, Nakanishi H et al. MicroRNA-31 predicts the presence of lymph node metastases and survival in patients with lung adenocarcinoma. *Clin Cancer Res* 2013; 19:5423-33; PMID:23946296; <http://dx.doi.org/10.1158/1078-0432.CCR-13-0320>
47. Dong Z, Zhong Z, Yang L, Wang S, Gong Z. MicroRNA-31 inhibits cisplatin-induced apoptosis in non-small cell lung cancer cells by regulating the drug transporter ABCB9. *Cancer Lett* 2014; 343:249-57; PMID:24099915; <http://dx.doi.org/10.1016/j.canlet.2013.09.034>
48. Zhong Z, Dong Z, Yang L, Chen X, Gong Z. MicroRNA-31-5p modulates cell cycle by targeting human mutL homolog 1 in human cancer cells. *Tumour Biol* 2013; 34:1959-65; PMID:23539435; <http://dx.doi.org/10.1007/s13277-013-0741-z>
49. Gao W, Liu L, Xu J, Shao Q, Liu Y, Zeng H, Shu Y. A systematic analysis of predicted MiR-31-targets identifies a diagnostic and prognostic signature for lung cancer. *Biomed Pharmacother* 2014; 68:419-27; PMID:24726065; <http://dx.doi.org/10.1016/j.biopha.2014.03.009>
50. Liu CJ, Tsai MM, Hung PS, Kao SY, Liu TY, Wu KJ, Chiou SH, Lin SC, Chang KW. miR-31 ablates expression of the HIF regulatory factor FIH to activate the HIF pathway in head and neck carcinoma. *Cancer Res* 2010; 70:1635-44; PMID:20145132; <http://dx.doi.org/10.1158/0008-5472.CAN-09-2291>
51. Olson P, Lu J, Zhang H, Shai A, Chun MG, Wang Y, Libutti SK, Nakakura EK, Golub TR, Hanahan D. MicroRNA dynamics in the stages of tumorigenesis correlate with hallmark capabilities of cancer. *Genes Dev* 2009; 23:2152-65; PMID:19759263; <http://dx.doi.org/10.1101/gad.1820109>
52. Hiratsuka S, Watanabe A, Aburatani H, Maru Y. Tumour-mediated upregulation of chemoattractants and recruitment of myeloid cells predetermines lung metastasis. *Nat Cell Biol* 2006; 8:1369-75; PMID:17128264; <http://dx.doi.org/10.1038/ncb1507>
53. Hiratsuka S, Ishibashi S, Tomita T, Watanabe A, Akashi-Takamura S, Murakami M, Kijima H, Miyake K, Aburatani H, Maru Y. Primary tumours modulate innate immune signalling to create pre-metastatic vascular hyperpermeability foci. *Nat Commun* 2013; 4:1853; PMID:23673638; <http://dx.doi.org/10.1038/ncomms2856>
54. Hsu YL, Hung JY, Tsai EM, Wu CY, Ho YW, Jian SF, Yen MC, Chang WA, Hou MF, Kuo PL. Benzyl butyl phthalate increases the chemoresistance to doxorubicin/cyclophosphamide by increasing breast cancer-associated dendritic cell-derived CXCL1/GROalpha and S100A8/A9. *Oncol Rep* 2015; 34:2889-900; PMID:26397389; <http://dx.doi.org/10.3892/or.2015.4307>
55. Cheng P, Corzo CA, Luetsteke N, Yu B, Nagaraj S, Bui MM, Ortiz M, Nacken W, Sorg C, Vogl T et al. Inhibition of dendritic cell differentiation and accumulation of myeloid-derived suppressor cells in cancer is regulated by S100A9 protein. *J Exp Med* 2008; 205:2235-49; PMID:18809714; <http://dx.doi.org/10.1084/jem.20080132>
56. Feng PH, Lee KY, Chang YL, Chan YF, Kuo LW, Lin TY, Chung FT, Kuo CS, Yu CT, Lin SM et al. CD14(+)/S100A9(+) monocytic myeloid-derived suppressor cells and their clinical relevance in non-small cell lung cancer. *Am J Respir Critical Care Med* 2012; 186:1025-36; PMID:22955317; <http://dx.doi.org/10.1164/rccm.201204-0636OC>
57. Xia B, Herbst RS. Immune checkpoint therapy for non-small-cell lung cancer: an update. *Immunotherapy* 2016; 8:279-98; PMID:26860624; <http://dx.doi.org/10.2217/imt.15.123>
58. Lutz MB, Kukutsch N, Ogilvie AL, Rossner S, Koch F, Romani N, Schuler G. An advanced culture method for generating large quantities of highly pure dendritic cells from mouse bone marrow. *J Immunol Methods* 1999; 223:77-92; PMID:10037236; [http://dx.doi.org/10.1016/S0022-1759\(98\)00204-X](http://dx.doi.org/10.1016/S0022-1759(98)00204-X)
59. Subramanian A, Tamayo P, Mootha VK, Mukherjee S, Ebert BL, Gillette MA, Paulovich A, Pomeroy SL, Golub TR, Lander ES et al. Gene set enrichment analysis: a knowledge-based approach for interpreting genome-wide expression profiles. *Proc Natl Acad Sci USA* 2005; 102:15545-50; PMID:16199517; <http://dx.doi.org/10.1073/pnas.0506580102>
60. Mootha VK, Lindgren CM, Eriksson KF, Subramanian A, Sihag S, Lehar J, Puigserver P, Carlsson E, Ridderstråle M, Laurila E et al. PGC-1alpha-responsive genes involved in oxidative phosphorylation are coordinately downregulated in human diabetes. *Nat Genet* 2003; 34:267-73; PMID:12808457; <http://dx.doi.org/10.1038/ng1180>
61. Mestdagh P, Feys T, Bernard N, Guenther S, Chen C, Speleman F, Vandesompele J. High-throughput stem-loop RT-qPCR miRNA expression profiling using minute amounts of input RNA. *Nucleic Acids Res* 2008; 36:e143; PMID:18940866; <http://dx.doi.org/10.1093/nar/gkn725>
62. Mestdagh P, Van Vlierberghe P, De Weer A, Muth D, Westermann F, Speleman F, Vandesompele J. A novel and universal method for microRNA RT-qPCR data normalization. *Genome Biol* 2009; 10:R64; PMID:19531210; <http://dx.doi.org/10.1186/gb-2009-10-6-r64>
63. De Wever O, Hendrix A, De Boeck A, Westbroek W, Braems G, Emami S, Sabbah M, Gespach C, Bracke M. Modeling and quantification of cancer cell invasion through collagen type I matrices. *Int J Dev Biol* 2010; 54:887-96; PMID:19757378; <http://dx.doi.org/10.1387/ijdb.092948ow>